Engineering Failure Analysis 163 (2024) 108462

Contents lists available at ScienceDirect

Engineering Failure Analysis

journal homepage: www.elsevier.com/locate/engfailanal

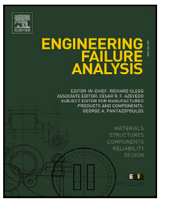

Collapse analysis of masonry arches and domes considering finite friction and uncertainties in compressive strength

Danila Aita *, Matteo Bruggi, Elsa Garavaglia

Department of Civil and Environmental Engineering, Politecnico di Milano, 20133, Milano, Italy

ARTICLE INFO

Keywords:
Masonry
Limit analysis
Arches and domes
Finite friction
Finite strength
Probabilistic analysis
Random variables
Probability of failure

ABSTRACT

Within the context of the lower bound theorem of classical limit analysis, the collapse of stone masonry arches and domes characterized by finite friction and uncertain finite compressive strength is addressed. Self-weight is considered, along with a live point load applied at the crown. A multi-constrained funicular approach based on the concept of force densities is implemented to provide the maximum static load multiplier for any assigned value of the friction coefficient and of the compressive strength. The numerical method, which takes into full account the stereotomy of blocky stone structures, is validated by using a novel version of the semi-analytical Durand-Claye's stability area method. Two different types of brickwork are considered in the investigation, addressing the compressive strength as a random variable with prescribed log-normal distributions. Due to the limited availability of data to elaborate probabilistic models for the angle of friction, the effect of this mechanical parameter on the probability of failure of the blocky structures is assessed by developing a set of fragility curves. For each discrete value in a representative range of friction coefficients, a Monte Carlo investigation is performed by iteratively applying the funicular method considering samples of the random variable that describes the compressive strength. The retrieved load multipliers are processed to estimate the probability of failure for any given magnitude of live load, which depends on the value of the friction coefficient. An insight into the collapse modes occurring in the masonry arches and domes under examination is provided, as well.

1. Introduction

Investigating the collapse behavior of unreinforced masonry vaults, such as arches and domes, represents a topical issue due to the complex mechanical response of masonry, a heterogeneous material characterized by a good compressive strength and a low tensile strength.

The challenges in conducting advanced experimental tests to determine masonry properties are described, for example, in [1], where the most relevant property in order to characterize this material is recognized to be the compressive strength in the direction normal to the bed joints separating the blocks. Among other contributions on this topic, [2] examine and compare different formulas to predict the compressive strength of masonry, starting from the characteristics of the elements composing the brickwork, while [3] assess the suitability of some experimental investigations aimed at determining the compressive strength by testing bricks and mortar, separately, or testing cylindrical cores. Some studies are focused on experimentally determining other material properties, such as the friction coefficient. Among them [4] study dry stack stone masonry constructions, by focusing on the assessment of the joint normal and shear stiffness along with friction parameters.

* Corresponding author.
E-mail address: danila.aita@polimi.it (D. Aita).

https://doi.org/10.1016/j.engfailanal.2024.108462
Received 14 February 2024; Received in revised form 25 April 2024; Accepted 16 May 2024
Available online 18 May 2024
1350-6307/© 2024 The Authors. Published by Elsevier Ltd. This is an open access article under the CC BY license (http://creativecommons.org/licenses/by/4.0/).

Faced with this complexity, probabilistic analyses are commonly adopted in order to capture the mechanical properties of masonry as well as the response of masonry structures. Without claiming completeness, some significant studies can be cited. As an example, the research conducted by [5] shows that compressive tests of masonry specimen under vertical constant load are affected by time, by highlighting that vertical and horizontal deformation increases according to three phases of creep. The authors deal with such a problem by means of a probabilistic analysis and suggest an experimental procedure capable of capturing the laboratory creep behavior; moreover, they propose a probabilistic approach for the estimate of the residual life of the material. In the contribution by [6], the fragility curves method is proposed as an agile tool, able to predict the evolution of deterioration process for masonry structures, while [7] propose a stochastic analysis based on Monte Carlo simulation for the seismic assessment of historical masonry structures by considering the uncertainty of masonry parameters. The analysis by [8] presents a probabilistic-based numerical strategy in order to study masonry structures in the inelastic range, under a seismic load, by considering a propagation of uncertainty through loading, material, mechanical, and geometrical parameters; moreover, a random mechanical response of masonry is provided by means of a numerical homogenization procedure. As regards geometrical uncertainties, [9] study the collapse of circular masonry arches in the presence of horizontal seismic actions, by considering the influence of shape irregularities by means of a random generative model. For an overview on the failure analysis and performance of masonry and historical structures, by considering extreme events, degradation mechanisms, structural health monitoring techniques, and service life design approaches, the interested reader is addressed to [10,11].

Focusing on the behavior of masonry structures, different approaches are adopted nowadays, depending on the objectives of the analysis. Among the variety of contributions, we can observe that, on the one hand, there are finite element methods or discrete element methods, which introduce contact, friction and cohesion models implemented "ad hoc" in order to capture a realistic behavior of such structures [12–14]. On the other hand, there is a need for fast analysis methods capable of evaluating the overall stability or load-bearing capacity of masonry structures; in this context the role of optimization algorithms based on Limit Analysis [15–17] is particularly significant.

As regards the objective of this contribution, the simplest modeling of masonry vaults in the context of classical Limit Analysis describes these structures as an assembly of rigid blocks, with infinite compressive strength and zero tensile strength, due to the low, uncertain, tensile strength of the material, assuming an infinite coefficient of friction between the blocks [18]. These are the hypotheses on the masonry material proposed by Heyman's pioneering work [19], which captures a fundamental characteristic, i.e. its unilateral behavior, and provides an interpretative criterion of cracking patterns. Starting from these assumptions, modern re-visitations of graphical approaches [20] or sophisticated static methods have been developed [21–25]. With reference to the topic of this contribution, the minimum thrust analysis of axisymmetric masonry domes performed by [26–28] can be recalled.

It should be observed, however, that in real masonry structures the compressive strength as well as the friction coefficient are finite, so that crushing and sliding can occur. Adopting Heyman's hypotheses, therefore, could lead to unsafe solutions. A discussion on those contributions aimed at enriching Heyman's hypotheses in the framework of Limit Analysis by considering the effects of a limited compressive strength as well as of a limited friction coefficient on the collapse behavior of masonry vaults is out of the scope of the current paper. Without pretending to be exhaustive, we can cite [16,29–32], which introduce a limited friction coefficient, [17,33,34], which focus on the influence of strength requirements on the mechanical response of masonry vaults, and the analyses proposed by [35,36], where both strength and friction requirements are taken into account.

Given the above, the current study aims at exploring the collapse behavior of masonry arches and domes by means of an integrated method based on both deterministic lower bound approach, and a probabilistic investigation in order to assess the influence of a limited friction coefficient along with the uncertainty characterizing the compressive strength on the collapse behavior of such structures.

The research is focused on symmetric masonry arches and axi-symmetric domes of revolution subjected to self-weight and a vertical point load at the crown, assumed as a live load. This typology of structures is chosen since symmetry and geometric characteristics allow for finding the collapse load multiplier using procedures based on the lower bound theorem of Limit Analysis, even under the hypothesis of a finite friction coefficient. In this regard, it is worth remembering that, if friction is finite, the material presents non-standard plastic behavior, since any two adjacent voussoirs can slide relative to each other by violating the normality rule [37–41]. The case studies examined in this discussion belong to a class of problems for which the uniqueness of the solution is guaranteed, as well as the possibility of determining safe stress states. For further insights on this topic, the reader is referred to [39,42,43].

The analysis is developed by exploiting a funicular method based on the concept of force density [15,44,45], and a novel version of Durand-Claye's stability area method [17,36,46,47]. The funicular method allows one for finding the collapse load multiplier by solving a multi-constrained maximization problem. A three-dimensional network consisting of branches subjected to axial forces is considered. The nodes are situated along vertical straight lines passing through the centers of gravity of each of the blocks composing the vault. Considering a fixed plan projection and local constraints, applied at each joint, the maximization procedure allows the maximum static load multiplier to be obtained for a given friction coefficient and a given compressive strength. The results thus obtained are validated using the semi-analytical Durand-Claye method: in this case an iterative procedure is necessary to find – with the desired precision – the load multiplier corresponding to the limit condition, i.e., to the vanishing of the stability area.

As is well known, deterministic limit analysis does not take adequately into account the influence of the uncertainties on the stability of masonry structures. In this contribution, the uncertainty related to the estimation of the material compressive strength is considered. Two different materials are examined, assuming the strength in compression as a random variable characterized by log-normal distributions, see technical documents [48]. A realistic representation of the influence of material parameters would also require considering the friction coefficient as a random variable. However, the availability of data to elaborate probabilistic models

for the friction coefficient is limited. In [49], an experimental characterization of dry masonry joints was performed depending on the surface roughness of the blocks, thus defining an interval of friction coefficients that is representative of a wide range of situations. Since the compressive strength can be effectively described as a random variable, but this is not a viable option for the friction coefficient, the effect of the latter parameter on the probability of failure of dry blocky structures is herein addressed by resorting to the concept of fragility curves. In the probabilistic seismic performance assessment of structures and seismic risk analysis, a collapse fragility curve provides the probability of failure given a certain seismic intensity measure, see e.g. [50] and [7]. Following [6], the same tool can be exploited to represent the probability of failure given a certain load intensity measure, i.e. a multiplier of the applied load. Hence, looking at a set of fragility curves which are retrieved for different discrete values of the friction coefficient, the impact of such mechanical parameter on the structural safety can be preliminary investigated without the need to handle the friction angle as a random variable. A Monte Carlo analysis is performed by iteratively applying the funicular method to masonry arches and vaults assuming samples of the compressive strength, while spanning the representative interval of friction coefficients reported in the experimental characterization by [49]. Given a friction coefficient, the computed load multipliers are handled as a random variable, thus allowing for an estimation of the probability of failure for any prescribed magnitude of the live load. The achieved results are commented on, elaborating on collapse modes that occur in the examined masonry arches and domes.

The remainder of this paper is organized as follows. In Section 2 the limit analysis by means of the force density method and mathematical programming is presented. An overview of the forces, eccentricities, and constraints at the joints is given, along with details of the optimization problem. In Section 3 the Durand-Claye method is discussed, focusing on the procedure implemented to find the load multiplier for symmetric arches and domes corresponding to the limit condition, i.e., to the vanishing of the stability area. In Section 4 the probabilistic investigation is introduced and the achieved numerical results are presented and commented on, pointing out the role of friction both in terms of collapse mode and expected failure probabilities for given loads. Finally, Section 5 provides concluding remarks, along with directions for further research.

2. Limit analysis using funicular networks and mathematical programming

The equilibrium of arches and domes is investigated by means of an approach of funicular analysis [51] that relies on the "force density method" [44]. Given a Cartesian reference system $Oxyz$, any three-dimensional network consists of m elements and n_s nodes, whose coordinates are stored in the arrays $\mathbf{x}_s$, $\mathbf{y}_s$, and $\mathbf{z}_s$. The topology of the spatial network is described by the connectivity matrix $\mathbf{C}_s$, being $\mathbf{C}$ the subset which corresponds to the unrestrained nodes, while $\mathbf{C}_f$ refers to the restrained ones. Accordingly, one has $\mathbf{u} = \mathbf{C}_s\mathbf{x}_s$, $\mathbf{v} = \mathbf{C}_s\mathbf{y}_s$, and $\mathbf{w} = \mathbf{C}_s\mathbf{z}_s$, where $\mathbf{u}$, $\mathbf{v}$, and $\mathbf{w}$ collect the differences in coordinates between the ends of each element along the x, y, and z axes, respectively. The array gathering the length of the members of the network is denoted by $\mathbf{l}$, with $l_i = \sqrt{u_i^2 + v_i^2 + w_i^2}$, whereas $\mathbf{s}$ collects the branch forces. Upon introduction of $\mathbf{L} = \mathrm{diag}(\mathbf{l})$, the force density array reads $\mathbf{q} = \mathbf{L}^{-1}\mathbf{s}$, which stores the force-to-length ratios of the members of the network. In this study, networks with a fixed plan projection subjected to vertical forces only are considered, see, e.g. [52–54]. Hence, the horizontal equilibrium of the unrestrained nodes reads:

$$\begin{bmatrix} \mathbf{C}^T \mathrm{diag}(\mathbf{C}_s\mathbf{x}_{s0}) \\ \mathbf{C}^T \mathrm{diag}(\mathbf{C}_s\mathbf{y}_{s0}) \end{bmatrix} \mathbf{q} = \begin{bmatrix} \mathbf{0} \\ \mathbf{0} \end{bmatrix}, \tag{1}$$

where $\mathbf{x}_{s0}$ and $\mathbf{y}_{s0}$ collect the prescribed x and y coordinates of the nodes. Eq. (1) implies that $m - r$ independent force densities exist, stored in $\overline{\mathbf{q}}$, being r the rank of the coefficient matrix. The r dependent force densities read $\widetilde{\mathbf{q}} = \mathbf{B}\overline{\mathbf{q}} + \mathbf{d}$, where $\mathbf{B}$ and $\mathbf{d}$ are found by performing Gauss–Jordan elimination on Eq. (1), see in particular [53]. Upon introduction of $\mathbf{Q} = \mathrm{diag}(\mathbf{q})$, the equilibrium along the vertical axis may be written as:

$$\mathbf{C}^T\mathbf{Q}\mathbf{C}\mathbf{z} + \mathbf{C}^T\mathbf{Q}\mathbf{C}_f\mathbf{z}_f = \mathbf{p}_z, \quad \text{with} \quad \mathbf{p}_z = \mathbf{p}_{zd} + \lambda\mathbf{p}_{zl}. \tag{2}$$

In the above equation, $\mathbf{z}$ represents the subset of $\mathbf{z}_s$ related to the unrestrained nodes, whereas $\mathbf{z}_f$ pertains to the restrained ones. The load vector $\mathbf{p}_z$ is made by the dead load $\mathbf{p}_{zd}$ and the live load $\mathbf{p}_{zl}$, being the latter scaled by the multiplier λ. For any given set of $\overline{\mathbf{q}}$ and $\mathbf{z}_f$, along with prescribed loads, Eq. (2) allows one for calculating the vertical coordinates of the unrestrained nodes of the funicular network.

The nodes of the network are chosen so that they lie on the vertical straight lines passing through the centroids of the voussoirs, see Fig. 1. The members of the network intersect the planes of the joints which separate adjacent blocks, see Fig. 2. Denoting by $\mathbf{e}_x$, $\mathbf{e}_y$, and $\mathbf{e}_z$ the unit vectors aligned with the x, y, and z directions, respectively, the funicular force $\mathbf{F}_i$ reads:

$$\mathbf{F}_i = q_i \left(u_i\,\mathbf{e}_x + v_i\,\mathbf{e}_y + w_i\,\mathbf{e}_z \right). \tag{3}$$

The line of action of $\mathbf{F}_i$ crosses the ith joint at point P_i, while C_i represents the centroid of the joint. Rectangular sections are used as a simplification in this contribution. The principal axes of inertia are denoted as $\boldsymbol{\xi}_i$ and $\boldsymbol{\eta}_i$, whereas $\mathbf{n}_i$ is the normal vector. The size of the rectangular section is $l_{i,\xi} \times l_{i,\eta}$.

The magnitude of the normal component of $\mathbf{F}_i$, referred to as $\mathbf{N}_i$, can be found as $N_i = \mathbf{F}_i \cdot \mathbf{n}_i$. Its eccentricity with respect to $\boldsymbol{\xi}_i$ can be computed by evaluating the moment of $\mathbf{N}_i$ about the same axis, $M_{i,\xi}$, and scaling by N_i. Due to the fact that the shear component of $\mathbf{F}_i$ does not provide any contribution to $M_{i,\xi}$, one has:

$$e_{i,\xi} = \mathrm{abs}\left(\frac{M_{i,\xi}}{N_i}\right), \text{with} \quad \frac{M_{i,\xi}}{N_i} = \frac{\boldsymbol{\xi}_i \cdot (\mathbf{r}_i \times \mathbf{F}_i)}{N_i}, \tag{4}$$

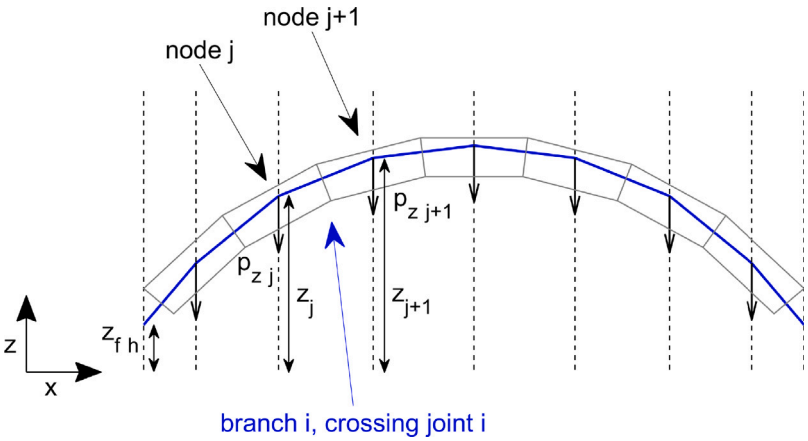

Fig. 1. Funicular network, with fixed plan projection, for a blocky stone structure.

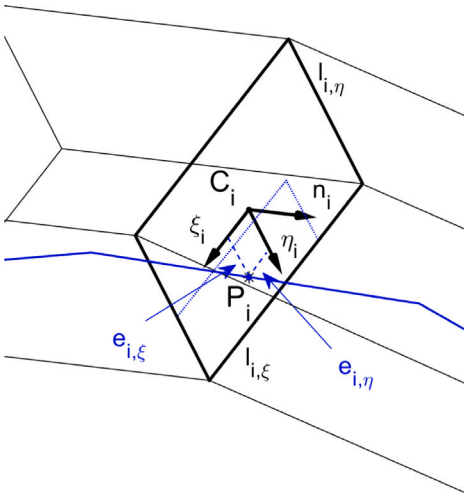

Fig. 2. The ith joint between two adjacent voussoirs.

where abs(·) is the absolute value of the scalar argument, while $\mathbf{r}_i$ is the vector drawn from C_i to any of the vertices of the ith member of the funicular network, both belonging to the line of action of $\mathbf{F}_i$. Similarly, the eccentricity of $\mathbf{N}_i$ with respect to $\boldsymbol{\eta}_i$ is:

$$e_{i,\eta} = \text{abs}\left(\frac{M_{i,\eta}}{N_i}\right), \text{with } \frac{M_{i,\eta}}{N_i} = \frac{\boldsymbol{\eta}_i \cdot (\mathbf{r}_i \times \mathbf{F}_i)}{N_i}. \tag{5}$$

Moreover, the magnitude of the shear component of $\mathbf{F}_i$, referred to as $\mathbf{V}_i$, may be found as the modulus of the vector difference $\mathbf{F}_i - \mathbf{N}_i$. This implies:

$$V_i^2 = \left(q_i\, u_i - N_i\, n_{i,x}\right)^2 + \left(q_i\, v_i - N_i\, n_{i,y}\right)^2 + \left(q_i\, w_i - N_i\, n_{i,z}\right)^2. \tag{6}$$

In this contribution, symmetric structures that are symmetrically loaded are considered. For this reason, the twisting moment resulting from the eccentricity of $\mathbf{V}_i$ is disregarded.

A multi-constrained optimization problem can be formulated to maximize the load multiplier λ searching among the set of funicular networks that fulfill equilibrium along with prescribed limit conditions at the joints. The following statement is

implemented:

$$\begin{cases} \max\limits_{\substack{\lambda>0 \\ \overline{\mathbf{q}}\leq\mathbf{0} \\ \mathbf{z}_f^{min}\leq\mathbf{z}_f\leq\mathbf{z}_f^{max}}} \lambda & \text{(a)} \\ \text{s.t.} & \\ \widetilde{\mathbf{q}} = \mathbf{B}\overline{\mathbf{q}} + \mathbf{d}, & \text{(b)} \\ \mathbf{C}^T\mathbf{Q}\mathbf{C}\mathbf{z} + \mathbf{C}^T\mathbf{Q}\mathbf{C}_f\mathbf{z}_f = \mathbf{p}_z(\lambda), & \text{(c)} \\ \widetilde{q}_k \leq 0, \quad \text{for } k = 1...r, & \text{(d)} \\ \frac{N_i}{-\sigma_c\left(l_{i,\xi}-2e_{i,\eta}\right)\left(l_{i,\eta}-2e_{i,\xi}\right)} \leq 1, \quad \text{for } i = 1...m, & \text{(e)} \\ \frac{V_i^2}{\left(N_i\tan\psi\right)^2} \leq 1, \quad \text{for } i = 1...m. & \text{(f)} \end{cases} \tag{7}$$

The independent force densities $\overline{\mathbf{q}}$ and the vertical coordinates of the restrained nodes $\mathbf{z}_f$ are the sets of unknowns that, for any given load multiplier λ, govern the funicular equilibrium, see Eq. (7b) for the horizontal directions and Eq. (7c) for the vertical one. The arising of any positive force density is prevented because of the side enforcements on $\widetilde{\mathbf{q}}$ and the set of local constraints in Eq. (7d). Denoting by $\sigma_c \geq 0$ the strength in compression, Eq. (7e) ensures that crushing is prevented at the ith no-tension joint. According to the adopted strength criterion, a uniform distribution of compressive stresses in the area with size $\left(l_{i,\xi} - 2e_{i,\eta}\right) \times \left(l_{i,\eta} - 2e_{i,\xi}\right)$ is assumed to withstand the eccentric axial force N_i, see in particular [33,46]. Upon introduction of the friction angle ψ, Eq. (7f) prevents sliding at the ith joint, by imposing that the ratio V_i to N_i obeys the Coulomb's law [55]. In case the torsional capacity of the frictional interfaces has to be dealt with, Eq. (7) can be endowed with some relevant constraints, see in particular [56]. Alternatively, Eqs. (7e) and (7f) can be replaced by limit functions that account for interactions of the torsional strength with shear forces and bending moments, see e.g. [57]. In the presented numerical study it is assumed that failure may occur due to the attainment of limit conditions that involve the joints only, meaning that no additional enforcement is implemented for the voussoirs. Indeed, the constraints implemented in [45] to control the vertical coordinates of the nodes of the funicular network are herein disregarded.

As discussed in [15], problems in the form of Eq. (7) can be handled by sequential convex programming, exploiting gradient-based methods that were originally conceived for solving optimization problems for elastic structures, see also [58]. Compared to the minimum thrust problems solved in [15,45], sensitivities with respect to the load multiplier are also needed to handle Eq. (7). Looking at Eq. (2), the derivative of $\mathbf{z}$ with respect to λ may be straightforwardly computed as:

$$\frac{\partial\mathbf{z}}{\partial\lambda} = \left(\mathbf{C}^T\mathbf{Q}\mathbf{C}\right)^{-1}\mathbf{p}_{zl}. \tag{8}$$

For the numerical investigation presented in Section 4, the Method of Moving Asymptotes (MMA) [59] was employed. A validation of the implemented framework was preliminary performed by comparing results of benchmark simulations against the semi-analytical Durand-Claye's method [60,61] that is presented next.

3. Limit analysis using a novel version of the stability area method

In this section, another approach based on the lower bound theorem of limit analysis is described, namely a modern version of the Durand-Claye method [60,61], also known as the stability area method. This procedure, which can be defined as semi-analytical, is adopted here both to validate the results obtained through the funicular numerical method and to easily derive numerical outcomes when some parameters are fixed, while others are variable. Reference will be made to the revised version of this method developed by [17,36,46,47], with the aim of determining the maximum value of the static load multiplier, λ. The object of investigation are symmetric masonry arches and domes of revolution subjected to vertical loads, i.e., their self-weight and the weight of a crown point load acting downwards. The latter corresponds to $\lambda\mathbf{p}_{zl}$ in Eq. (2).

This method consists in imposing the equilibrium conditions for a portion of structure between the ideal vertical crown joint and any joint i (see Fig. 3). For a masonry arch, a constant out of plane thickness, t, is assumed; for an axi-symmetric dome, the method is similarly applied to a 'lune' of amplitude equal to $\Delta\phi$, which behaves as an independent half-arch with a variable width according to the so-called 'slicing technique' (see for example [62,63]). An absolute Cartesian coordinate system $Oxyz$ is adopted, according to which the (x, z) plane coincides with the vertical plane of symmetry containing the curved profile (with O belonging to the vertical symmetry axis, z, for the arch, to the axis of revolution, z, for the dome, see Fig. 3). Any joint i, defined by its co-latitude θ_i with respect to the z axis, is modeled as a rectangle, $l_{i,\eta} \times t$ for the arch, $l_{i,\eta} \times x_{C_i}\Delta\phi$ for the 'lune', where C_i is the midpoint of segment D_iE_i. The analyses related to masonry domes carried out in this paper by means of the Durand-Claye method, unless otherwise specified, are performed assuming this modeling for the joint. The vertical point load acting at the crown is set equal to $\lambda/n \times 1$ kN, where $n = 2$ for the (half) arch and $n = 2\pi/\Delta\phi$ for the dome's 'lune' (Fig. 3). By symmetry, a horizontal thrust, f, acts at the ideal vertical section. The center of pressure, P_0, see Fig. 3, identifies a positive eccentricity of f, denoted as e_0, with respect to the centroid C_0 of this section.

With reference to Fig. 4(left), the stability area A is the black region plotted in the (f, e_0) plane, which identifies the complete set of statically admissible solutions compatible with both equilibrium conditions and strength requirements at any joint i. Since

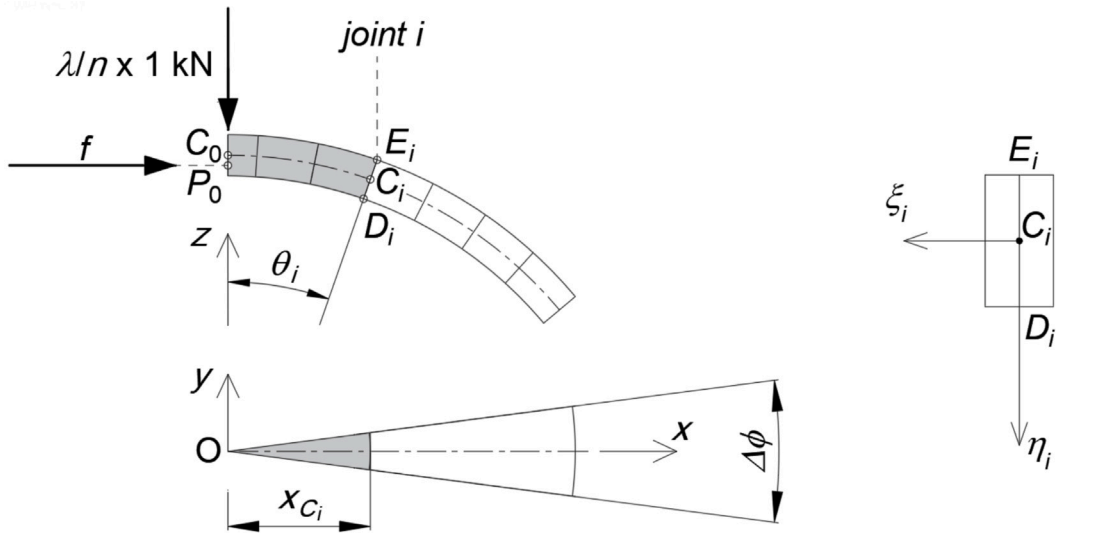

Fig. 3. Scheme of a masonry half arch (or dome's 'lune') subjected to its self-weight and to a vertical point load $\lambda/n \times 1$ kN at the crown (left); simplified geometry of the cross section (joint i) (right).

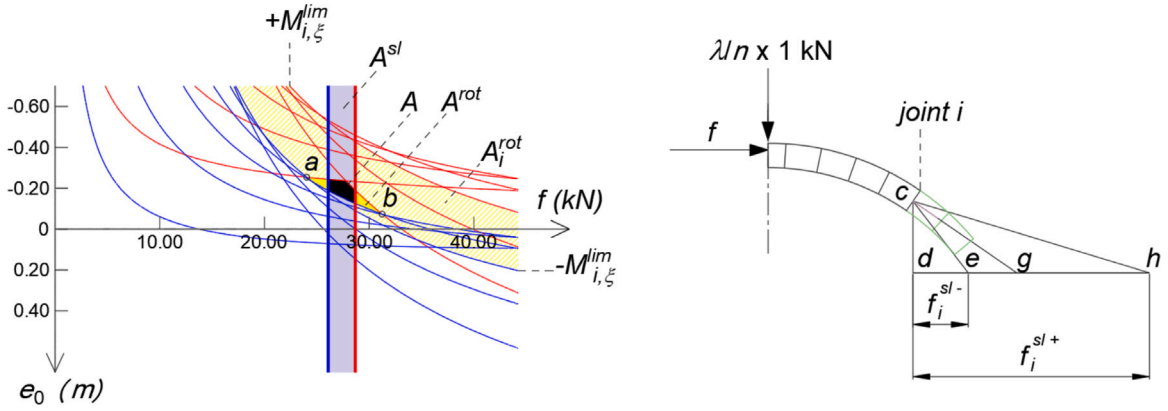

Fig. 4. The stability area related to an arch (left). Scheme of an arch (or 'lune') profile and of the triangles of forces defined by the friction angle (right).

a limited compressive strength, σ_c, is assumed as well as a limited friction coefficient, $\tan\psi$, the stability area A is obtained by intersecting the rotational domain, A^{rot}, with the sliding domain, A^{sl}, as will be better clarified later.

As already described in previous works [36,45], the graphical procedure can be re-interpreted in terms of internal forces. For the peculiar load conditions, $M_{i,\eta}$ is nil at any joint i, while the formal expressions of bending moment, $M_{i,\xi}$, and normal force, N_i, can be obtained by imposing the equilibrium conditions of the portion of structure under examination (see Fig. 3). For any joint i, the following holds:

$$M_{i,\xi} = M_{i,\xi}(f, e_0, \theta_i, \lambda) \text{ and } N_i = N_i(f, \theta_i, \lambda). \tag{9}$$

By considering the constraint imposed by Eq. (7e), $M^{lim}_{i,\xi}$ depends on the normal force, N_i, as well as the limited masonry compressive strength, σ_c:

$$M^{lim}_{i,\xi} = -\frac{N_i\left(N_i + l_{i,\xi}\, l_{i,\eta}\, \sigma_c\right)}{2\, l_{i,\xi}\, \sigma_c}. \tag{10}$$

In the (f, e_0) plane, the red and blue curves correspond to the attainment of $+M^{lim}_{i,\xi}$ and $-M^{lim}_{i,\xi}$ at any ith joint, respectively. For each joint i, the area A^{rot}_i (see the light yellow region in Fig. 4, left) is implicitly defined by the inequalities

$$-M^{lim}_{i,\xi} \le M_{i,\xi} \le +M^{lim}_{i,\xi}. \tag{11}$$

By repeating this procedure for all the joints i, and intersecting all the areas A^{rot}_i just defined, the rotational domain, A^{rot}, is obtained (see the solid yellow region identified by $a \le f \le b$ in Fig. 4, left).

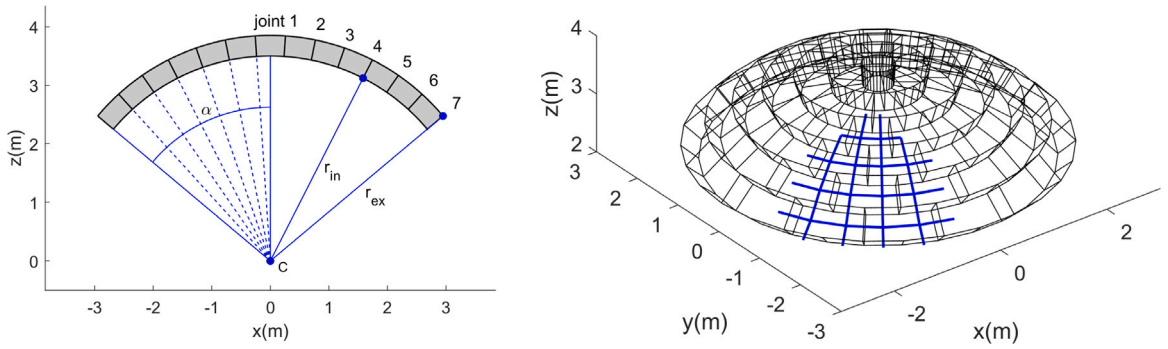

Fig. 5. Geometry and stereotomy of the considered arch (left) and dome (right).

Furthermore, in order to take into account the presence of an internal friction, the limit values of the crown thrust, $f_i^{sl\pm}$, related to any joint i, are determined by considering the equilibrium of the structure's portion comprised between the crown section and such a joint. The corresponding self-weight is denoted as W_i. Now, let us draw the triangles of forces cde, cdh, by assuming the assigned friction angle, ψ, and the resultant of the vertical loads, Q_i (corresponding to segment cd in the triangles of forces), obtained by summing the weight W_i and the crown point load ($\lambda/n \times 1$ kN). The following relations are obtained for $f_i^{sl\pm}$ (see the segments de, dh):

$$f_i^{sl\pm} = Q_i \tan\left(\pi/2 - \theta_i \pm \psi\right). \tag{12}$$

The sliding domain related to any joint i, A_i^{sl}, is defined by the conditions $f_i^{sl-} \le f_i \le f_i^{sl+}$. If the procedure is repeated for all the joints, the sliding domain, A^{sl}, is obtained, see the grey region in Fig. 4(left) bounded by two vertical straight lines. The area of stability A (see the black region) is the intersection between the rotational and sliding domains, A^{rot} and A^{sl}.

The modern version of the Durand-Claye method allows the collapse load multiplier to be determined with the desired precision using an iterative procedure. By incrementally increasing the value of λ, the stability area progressively decreases, until it disappears: this is the condition corresponding to the collapse. It is interesting to note that simply by observing the shape of the stability area and examining whether it is reduced to a single point or to a segment, the collapse mechanism that originates in the arch (or 'lune') is identified.

The examination of some case studies will provide additional details on this procedure.

4. Numerical investigations

A symmetric masonry arch and a dome acted upon by self-weight (dead load) and a vertical point force at the crown (live load) are considered. A material with a unit weight of $\gamma_m = 15$ kN/m^3 is assumed. The point load is specified as $\lambda \times 1$ kN, acting downwards.

The geometry and the stereotomy of the considered arch are represented in Fig. 5(left). The intrados lies along a circle centered at $C = (0, 0, 0)$ m, of radius $r_{in} = 3.50$ m. The extrados lies along a circle centered at the same point, of radius $r_{ex} = 3.85$ m. Half the angle of embracement, α, is 50°. The out-of-plane thickness of the arch is $t = 0.50$ m. The arch is made of thirteen voussoirs of amplitude 7.69°, whose stereotomy is defined by radial lines originating from point C.

The reference section of the dome of revolution is the same as the arch represented in Fig. 5(left). Here too, the arrangement of the voussoirs is defined by radial lines originating from the point C. Each of the thirty 'lunes' (with $\Delta\phi = 12°$ along the hoop direction) consists of six voussoirs (excluding the one at the top) with an amplitude of 7.69° along the meridian direction. In Fig. 5(right), the stereotomy of the dome is given, along with a sketch concerning the modeling of staggered voussoirs, see [45]. Each one of the voussoir is split into two sub-blocks, thus defining a pair of nodes of the funicular network. This allows for considering both meridian and hoop forces.

The strength in compression σ_c is given as a continuous random variable. Two different materials are considered, namely ashlars of soft stone (material A) and stone square blocks (material B). In both cases, log-normal distributions are assumed as suggested by [48], with parameters μ and s. The mean and the standard deviation of logarithmic values are assumed as $\mu_A = 0.0528$ MPa and $s_A = 0.0027$ MPa, when dealing with ashlars of soft stone, while $\mu_B = 0.0656$ MPa and $s_B = 0.0014$ MPa when addressing stone square blocks. The relevant probability density functions (PDFs) are plotted in Fig. 6.

In the experimental characterization of the Coulomb's failure criterion for dry masonry joints reported by [49] the friction coefficient, before sliding occurs, ranges in the interval $0.2 \le \tan\psi \le 0.6$, depending on the surface roughness. The lowest value was found to apply to a set of blocks with polished surface (using sandpaper), whereas the largest one was measured for blocks sawn mechanically. The latter case was characterized by a friction coefficient slightly larger than that derived for blocks with an artificially rough surface (created by a mechanically random spike).

To assess the effect of the variability of the friction angle when combined with the uncertainty on the strength in compression, the optimization approach presented in Section 2 is iteratively applied to one set of random values σ_c for each of the two log-normal

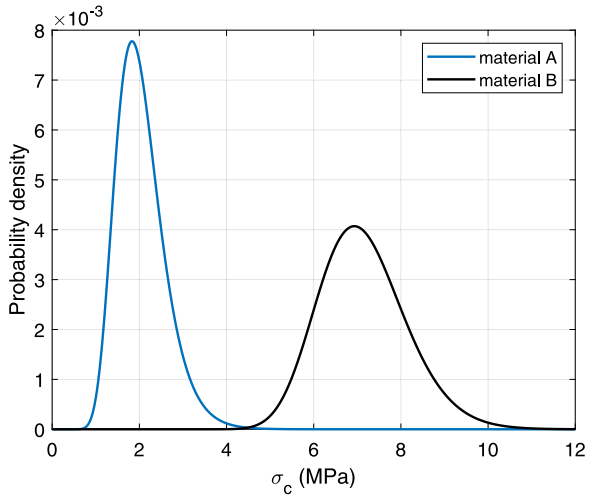

Fig. 6. Probability density functions adopted in the numerical studies for material A (ashlars of soft stone) and B (stone square blocks).

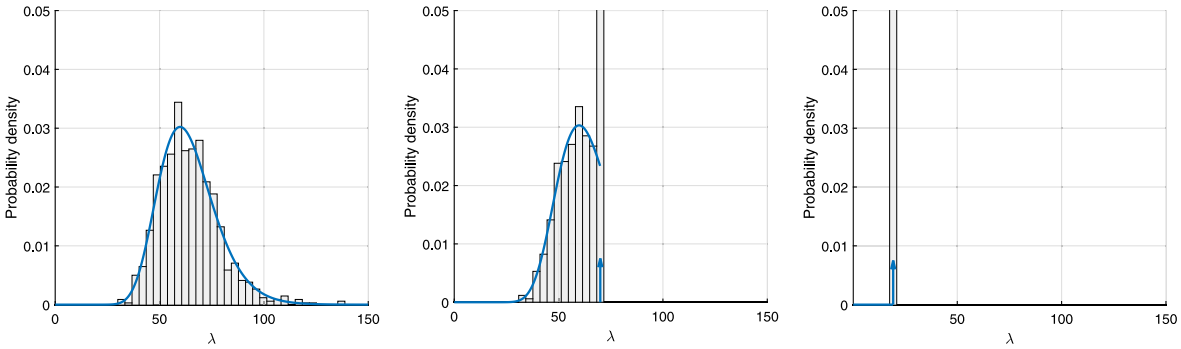

Fig. 7. Arch (material A). Normalized histogram and estimate of the probability density of the load multiplier for different values of the friction coefficient: $\tan\psi = 0.45$ (left), $\tan\psi = 0.38$ (center), and $\tan\psi = 0.3$ (right).

density functions in Fig. 6. The interval $0.2 \leq \tan\psi \leq 0.6$ is spanned by means of increments equal to 0.0025, for the arch, and equal to 0.005, for the dome. For each value of $\tan\psi$, the set of random values of the compressive strength has size 1000 for the arch, whereas 100 for the dome.

The probabilistic investigation will be presented in the next sections. Both for the arch and the dome, the output random variable will be analyzed to assess the behavior of the curved structures and estimate the probability of failure for any given value of the point loads. The optimization approach will be validated using the stability area method, see Section 3. While the funicular method is based on the resolution of an optimization problem aimed at maximizing the statically admissible load multiplier, an iterative application of Durand-Claye's method is needed to find λ: the load multiplier is progressively increased in order to identify the limit condition, which corresponds to the reduction of the stability area to a single point or to a segment, depending on the collapse mode thus identified.

The numerical analyses have been performed by means of appositely developed algorithms implemented in MATLAB [64] (funicular method) and in Mathematica [65] (Durand-Claye's method).

4.1. Arch

At first, material A is considered. In Fig. 7, normalized histograms are reported for three different values of the friction coefficient. In all the pictures, each bin provides the relative occurrence that a computed load multiplier falls within the range given by the bin width. The adopted estimate of the probability density function (PDF) is represented, as well.

For large values of the friction coefficient, say $\tan\psi \geq 0.4$, a log-normal density function, further referred to as $g(\lambda)$, is found to provide a reasonable estimation for the PDF of the continuous random variable λ, independently on $\tan\psi$. The relevant cumulative distribution function (CDF) will be denoted as $G(\lambda)$. To give an example, the case $\tan\psi = 0.45$ is illustrated in Fig. 7(left).

For intermediate values of the friction coefficient, say $0.3 < \tan\psi < 0.4$, histograms of the type represented in Fig. 7(center) are found. All of them are bounded from above by a load multiplier λ_k, having relative occurrence a_k. This suggests the adoption of

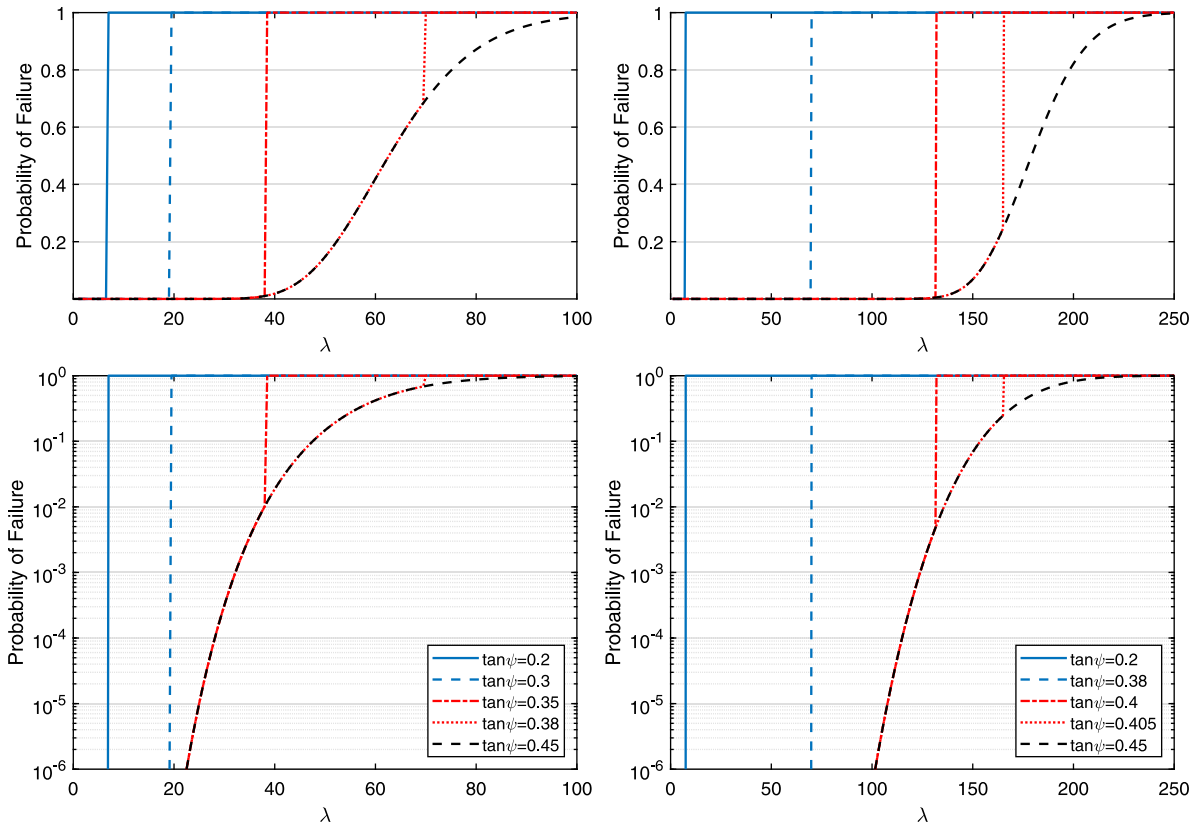

Fig. 8. Arch. Probability of failure vs. load multiplier for prescribed values of the friction coefficient: material A (left) and material B (right). The probability range is [0, 1] on top, whereas [10^{-6}, 1] below.

a mixed random variable to elaborate on the achieved results. An estimate of the relevant (generalized) PDF may be preliminary approximated by combining a truncated version of the log-normal density already used in the range $\tan\psi > 0.4$ and the Delta function $\delta(\lambda - \lambda_k)$. More in details, the function:

$$f(\lambda) = \begin{cases} g(\lambda) & \text{if } \lambda < \lambda_k, \\ b_k \delta(\lambda - \lambda_k) & \text{otherwise,} \end{cases} \tag{13}$$

is used, provided that the scaling factor b_k enforces $P(\lambda \leq \lambda_k) = 1$, i.e. $b_k = 1 - G(\lambda_k)$. The closer b_k to a_k, the higher is the affordability of the provided estimation. For the case depicted in Fig. 7(center), one has that $\lambda_k = 69.99$, with relative occurrence $a_k = 325/1000 = 0.325$, whereas $b_k = 0.304$.

Finally, for small values of the friction angle, that means $\tan\psi \leq 0.3$, the numerical investigation retrieves only one load multiplier per coefficient. This means that the load multiplier behaves as a discrete random variable. To preserve consistency with the model adopted above, Eq. (13) is used as the generalized PDF, implementing the same strategy to compute the scaling factor b_k. For instance, in the case $\tan\psi = 0.3$ of Fig. 7(right), the whole set of simulations provides the value $\lambda_k = 19.29$. The relative occurrence $a_k = 1$, whereas the adopted scaling factor is $b_k \sim 1$.

The probability of failure for a certain value of the load multiplier λ_m, incremented by any extremely small quantity, reads $P(\lambda \leq \lambda_m)$. Hence, given $\tan\psi$, when the PDF (either the generalized PDF) of the random variable λ is known, the probability of failure for a certain value of the (incremented) load multiplier λ_m is nothing but the CDF evaluated at λ_m. Diagrams reporting the probability of failure vs. the load multiplier can be conveniently built by constructing and evaluating CDFs for different values of $\tan\psi$. In Fig. 8, a few curves are provided both in the standard range [0, 1] (on top), and in the interval of interest for some engineering applications [10^{-6}, 1] (below). With reference to material A, see Fig. 8(left), for $\tan\psi \geq 0.4$, the diagram of the probability of failure is not affected in an appreciable manner by the value of the friction coefficient. In this range of $\tan\psi$, histograms are all equal to that shown in Fig. 7(left), meaning that $g(\lambda)$ applies. Hence, the cumulative distribution function of the load multiplier is the same, i.e. $G(\lambda)$. When the coefficient of friction is too small, there exists a certain value of λ, depending on $\tan\psi$, below which the structure is practically safe. Conversely, when the load multiplier exceeds such a value, failure is a sure event. For instance, when $\tan\psi = 0.3$, no equilibrium can be found for $\lambda > 19.29$, whereas below the structure may be considered safe. In between, the diagrams describing the probability of failure consist of a portion of the curve found for $\tan\psi \geq 0.4$, undergoing an abrupt change at a location that depends on $\tan\psi$. This is the case of $\tan\psi = 0.38$, for which failure becomes a sure event at $\lambda > 69.99$.

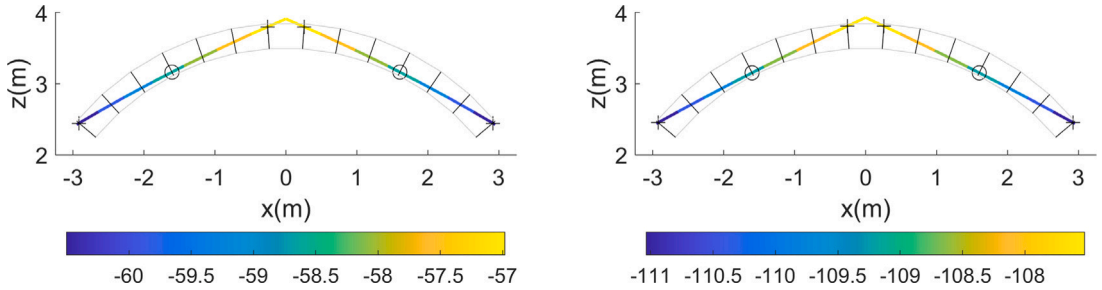

Fig. 9. Arch (material A). Funicular polygons at incipient collapse for $\tan\psi = 0.45$ and: $\sigma_{cA,0.05}$ ($\lambda = 44.30$) (left) and $\sigma_{cA,0.95}$ ($\lambda = 90.07$) (right). Forces are in kN.

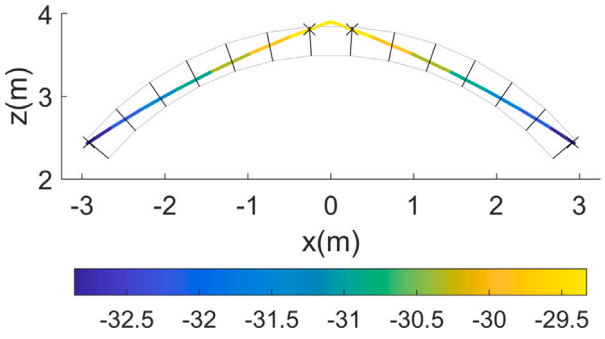

Fig. 10. Arch (material A). Funicular polygon at incipient collapse for $\tan\psi = 0.3$ and $\sigma_{cA,0.05}$ ($\lambda = 19.29$). Forces are in kN.

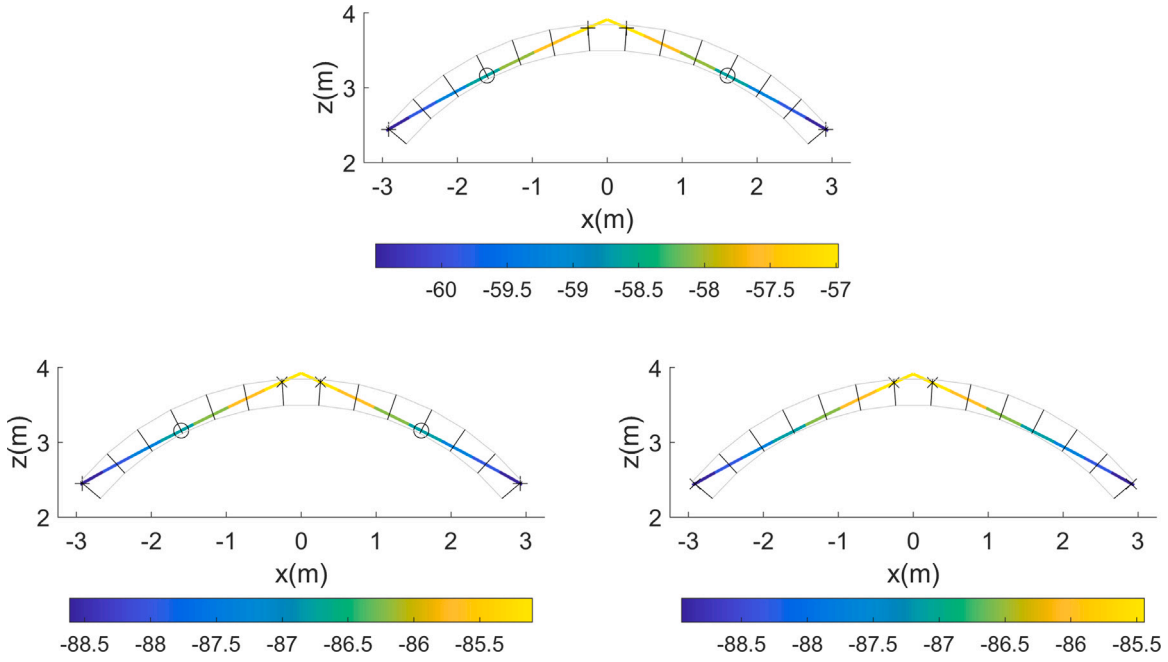

Fig. 11. Arch (material A). Funicular polygons at incipient collapse for $\tan\psi = 0.38$ and: $\sigma_{cA,0.05}$ ($\lambda = 44.30$) (top), $\sigma_{cA,0.69}$ ($\lambda = 69.70$) (bottom left), and $\sigma_{cA,0.95}$ ($\lambda = 69.99$) (bottom right). Forces are in kN.

To provide mechanical insight into the results presented in Fig. 7, load multipliers and relevant funicular polygons are addressed for the three cases of friction referenced above, considering two different values of the strength in compression each. These investigations are performed for $\sigma_{cA,0.05}$ = 1.26 MPa and $\sigma_{cA,0.95}$ = 3.07 MPa, which correspond to the fractile 5% and 95%, respectively, of the probability density function represented in Fig. 6 for material A.

In the pictures concerning funicular polygons/networks retrieved by Eq. (7), the symbols ° and + indicate joint sections where crossing members activate a strength constraint according to Eq. (7e), due to the assumptions of zero tensile strength and a limited compressive strength. The former symbol is used when the branch intersects the cross-section of the joint below the centroid, while the latter is used otherwise. The symbol × refers to any joint section whose crossing branch activates a friction constraint, according to Eq. (7f).

Funicular polygons at incipient collapse for $\tan\psi = 0.45$ are represented in Fig. 9. Coulomb's friction constraints are fulfilled all over the structure. Conversely, crossing members activate a strength constraint at three joints sections. Independently on the value of σ_c, the same critical joints are responsible for the incipient activation of a failure mechanism. The represented funicular polygons share the geometry, but different values of the collapse load multiplier are reported. The achieved results explain why, for large values of $\tan\psi$, the same distribution is observed for the continuous random variable λ, see Fig. 7(left). When $\tan\psi = 0.3$, the solution retrieved for $\sigma_{cA,0.05}$ coincides with that found for $\sigma_{cA,0.95}$, see Fig. 10. Strength constraints are fulfilled in all the joints. The activation of friction constraints both at the crown and at the imposts is responsible for the incipient activation of a purely sliding mechanism. For every small value of $\tan\psi$, only one load multiplier may be retrieved, see the description of λ as a discrete random variable when commenting on Fig. 7(right). The last set of investigations refers to the case $\tan\psi = 0.38$, see Fig. 11. For $\sigma_{cA,0.05}$, the same funicular polygon and load multiplier already found for $\tan\psi = 0.45$ are retrieved, see Fig. 9(left). For $\sigma_{cA,0.95}$, a funicular polygon of the type already found for $\tan\psi = 0.3$ (but larger value of the load multiplier) is reported, see Fig. 10. Indeed, the description of λ concerning results in Fig. 7(center) is that of a mixed random variable: the discrete part accounts for the cases in which the purely frictional collapse mode occurs, whereas the continuous one addresses failure modes that involve the activation of strength constraints. Since the same mode is observed for $\sigma_{cA,0.05}$ independently on $\tan\psi$, the truncated version of the PDF $g(\lambda)$ seems a reasonable model to preliminary address the continuous part of the mixed random variable. However, it must be pointed out that mixed strength/frictional modes may arise as well, see e.g. the result for $\sigma_{cA,0.69} = 2.25,$ MPa reported in Fig. 11.

In light of the above findings, an additional remark may be formulated with respect to the diagrams plotted in Fig. 8(left). The abscissa at which the abrupt change occurs, if any, is the load corresponding to the activation of a purely frictional collapse mode (for the relevant $\tan\psi$), that is λ_k of Eq. (13). For instance, looking at a probability of failure equal to 10^{-2}, a coefficient of friction that is slightly larger than 0.35 is needed to safely support $\lambda = 39.50$. For smaller values of $\tan\psi$, the probability of failure associated to the same load multiplier blows up due to the arising of a purely frictional collapse.

The numerical investigation presented above has been performed also for material B. In Fig. 8(right), diagrams giving the probability of failure vs. the load multiplier are constructed for different values of $\tan\psi$ (within the same ranges of probability already considered in the case of material A). As expected, for small values of $\tan\psi$, the load bearing capacity is the same, see e.g. the curve for $\tan\psi = 0.2$ in both pictures, crossing the λ axis at equal abscissa. In general, the compressive strength of material B allows for bearing larger loads, considering similar probabilities of failure, provided that the friction coefficient is such as to avoid the occurrence of a purely friction collapse.

In Fig. 12, curves representing λ_k, along with the maximum load multiplier computed for infinite σ_C, *versus* $\tan\psi$ are reported. It may be checked that the load multiplier λ_k, at which the abrupt change occurs in the fragility curves of Fig. 8, is the same as the maximum load multiplier computed for the relevant friction coefficient when assuming infinite compressive strength. This result, along with the finding that the continuous part of the probability density function in Eq. (13) is negligibly affected by the value of $\tan\psi$, suggests a simpler procedure to retrieve a set of fragility curves. A single Monte Carlo simulation, with no-sliding assumption, can be performed to recover the continuous part of the CDFs, whereas the computation of the collapse load multipliers for the considered friction coefficients, assuming infinite masonry compressive strength, provides the relevant values of λ_k, if any.

To validate the above results, a few comparisons are performed against the stability area method. In Fig. 9(left) an arch is plotted along with the funicular polygons at incipient collapse for $\tan\psi = 0.45$ and $\sigma_{cA,0.05}$. As observed before, the collapse load multiplier provided by the funicular method is $\lambda = 44.30$. In Fig. 13, the same arch is examined by means of Durand-Claye's method. In this case, the stability area reduces to a single point for a collapse load multiplier $\lambda_{DC} = 44.37$; more precisely, the stability area A (the black point in Fig. 13, left) corresponds to the intersection between the three curves $+M^{lim}_{1,\xi}$, $+M^{lim}_{7,\xi}$(red curves), and $-M^{lim}_{4,\xi}$ (blue curve), which highlights that a limit positive bending moment is reached at joints $i = 1$ and $i = 7$, while a limit negative bending value occurs at joint $i = 4$. It is interesting to observe that the stability area A is entirely contained in the sliding domain, see the region comprised between the two vertical straight lines colored light blue/light red in the (f, e_0) plane: in this case, collapse is due to the attainment of a limit condition linked only to the compressive and tensile strength requirements, according to the expression of the limit bending moment, given by Eq. (10), i.e., to the activation of strength constraints. The centers of pressure at these critical joints are marked with the same symbols adopted for the funicular method, i.e., the symbols + and ° indicate the attainment of positive/negative limit bending moment (Fig. 13, right).

Another comparison is performed in order to validate the results related to a purely sliding collapse mode. The same arch plotted in Fig. 10 is considered ($\tan\psi = 0.3$ and $\sigma_{cA,0.05}$; $\lambda = 19.29$). By means of Durand-Claye's method, it is observed that the stability area reduces to a vertical segment for $\lambda_{DC} = 19.35$, which corresponds to a limit condition related only to friction (see the black segment in Fig. 14, left), i.e., to the activation of friction constraints. Differently from the previous case study, an infinite set of thrust lines (Fig. 14, right) is identified, corresponding to a unique value of the crown thrust. The critical joints are indicated with the symbol ×. By considering the direction of the internal force at the critical joints with reference to the friction cone (Fig. 4, right), it is possible to capture the incipient collapse mechanism: at joint $i = 1$ (see the blue joint), downward sliding occurs, while at joint $i = 7$ (see the red joint) sliding is outwards.

In the examples just considered, the agreement with the results obtained via the funicular method is very good, both in terms of collapse load multiplier and critical joints.

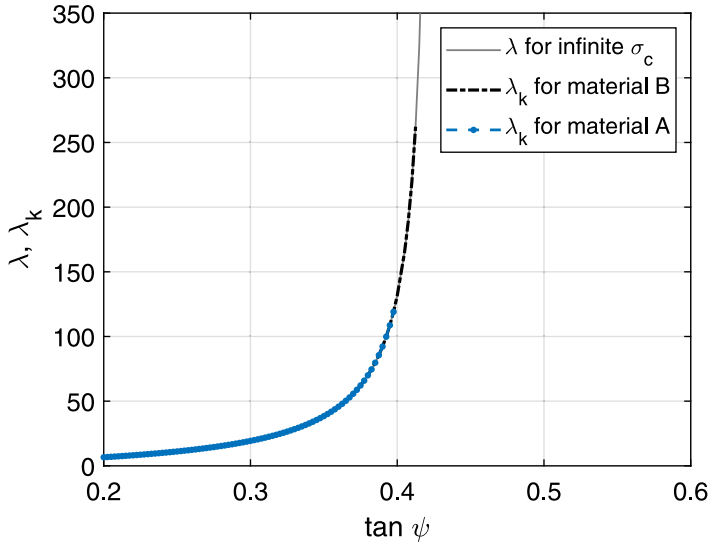

Fig. 12. Arch (materials A and B). Value of λ_k, along with the maximum load multiplier λ computed for infinite σ_C, *versus* friction coefficient $\tan\psi$.

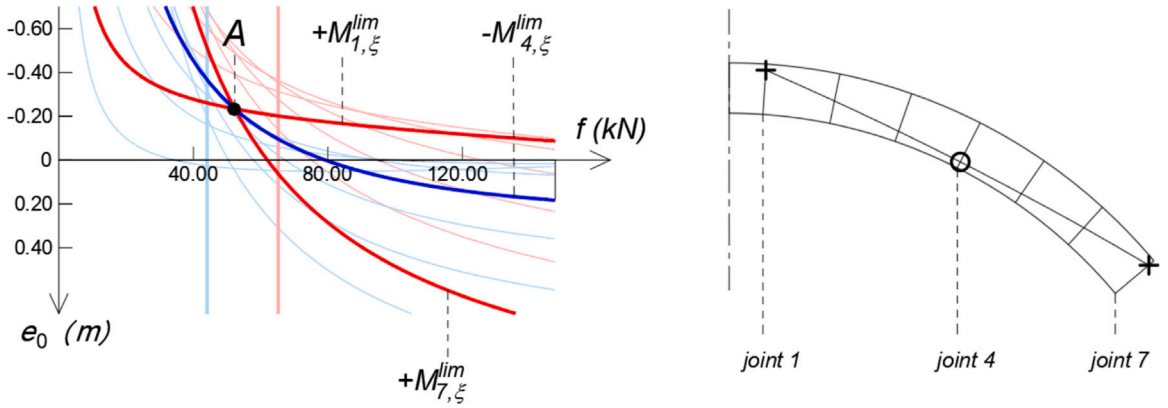

Fig. 13. Arch (material A). The stability area A reduces to a single point for $\tan\psi = 0.45$ and $\sigma_{cA,0.05}$ ($\lambda_{DC} = 44.37$) (left); the corresponding thrust line, with the location of the critical joints (right).

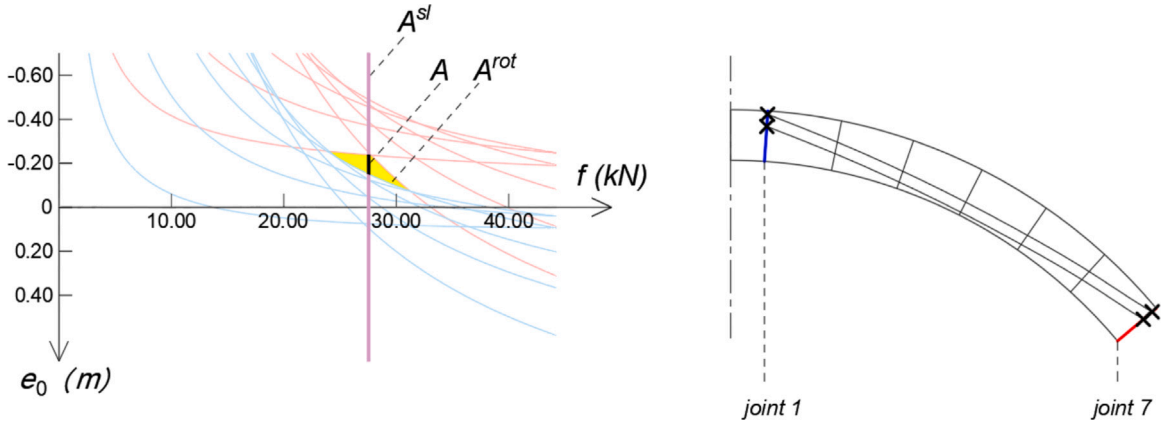

Fig. 14. Arch (material A). The stability area A reduces to a segment for $\tan\psi = 0.3$ and $\sigma_{cA,0.05}$ ($\lambda_{DC} = 19.35$) (left); the corresponding set of thrust lines, with the location of the critical joints (right).

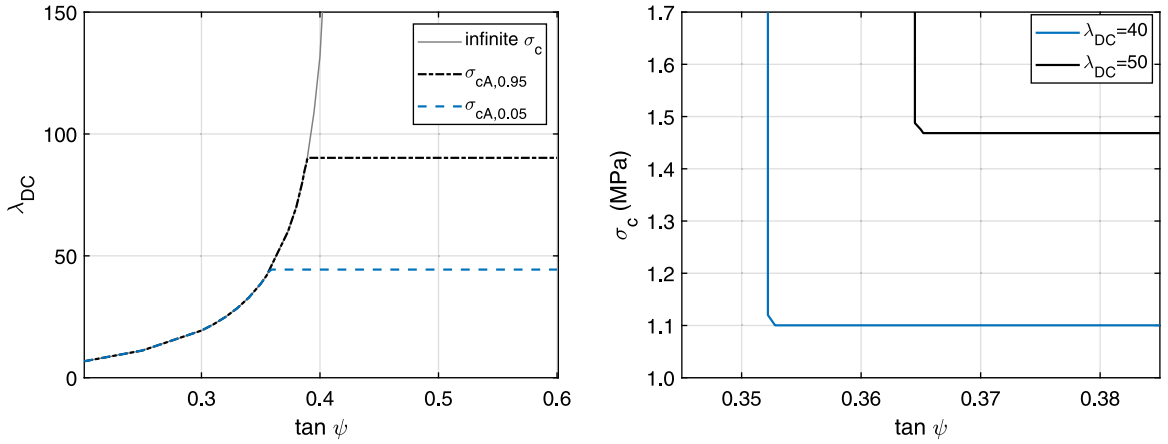

Fig. 15. Arch (material A). Maximum load multiplier, λ_{DC} *versus* friction coefficient, $\tan\psi$, for assigned values of the compressive strength (left); compressive strength corresponding to an incipient collapse condition, σ_c, *versus* friction coefficient, $\tan\psi$, for assigned values of λ_{DC} (right).

Given its semi-analytical formulation, the novel version of Durand-Claye's method is here exploited for performing deterministic analyses, which help clarify some results obtained through probabilistic investigation as well as the differences between a deterministic and probabilistic approach in Limit Analysis.

The first investigation consists in determining the collapse load multiplier, λ_{DC}, by varying the friction coefficient, while fixing the value of the compressive strength. In Fig. 15(left), a focus is provided on material A: three curves are plotted by assuming $\sigma_c = \sigma_{cA,0.05} = 1.26$ MPa, $\sigma_c = \sigma_{cA,0.95} = 3.07$ MPa, and infinite compressive strength. From the results, it emerges that the compressive strength affects the collapse modes arising in the arch by varying the friction coefficient. When $\sigma_c = \sigma_{cA,0.05} = 1.26$ MPa, for low values of the friction coefficient, $0.2 \le \tan\psi \le 0.358$, collapse occurs only due to the activation of friction constraints, which corresponds to the vanishing of the sliding domain. In this portion of the graph, the value of λ_{DC} dramatically increases with friction. A mixed collapse behavior, involving both friction and strength constraints, is found for $0.358 \le \tan\psi \le 0.359$. This range is very narrow and is not visible in the graph, due to the scaling factor adopted. For $0.359 \le \tan\psi \le 0.6$ the incipient collapse condition corresponds to the activation of only strength constraints, i.e., to the vanishing of the rotational domain. In this case, the value of the collapse load multiplier is constant while varying the friction coefficient, as testified by the horizontal trend. When $\sigma_c = \sigma_{cA,0.95} = 3.07$ MPa, a purely sliding collapse behavior occurs for $0.2 \le \tan\psi \le 0.389$. A mixed collapse behavior arises for a very narrow range of $\tan\psi$, i.e., for $0.389 \le \tan\psi \le 0.390$. A collapse related only to the activation of strength constraints emerges for $0.390 \le \tan\psi \le 0.6$. Note that the first portion of the graph (i.e., for $0.2 \le \tan\psi \le 0.358$) coincides with that obtained for $\sigma_{cA,0.05}$. Furthermore, for low values of the friction coefficient both of the graphs lie along the curve addressing the pure sliding modes that are found at infinite compressive strength.

Fig. 15(right) shows the results of a second investigation, i.e., by fixing the collapse load multiplier ($\lambda_{DC} = 40$ and $\lambda_{DC} = 50$) and varying the friction coefficient, $\tan\psi$, the compressive strength corresponding to a collapse condition is determined. Also in this case the transition from a sliding collapse mode to a rotational collapse mode is rather abrupt. In both graphs, the vertical portion, identified by $\tan\psi = 0.3522$ for $\lambda_{DC} = 40$, $\tan\psi = 0.3645$ for $\lambda_{DC} = 50$, corresponds to a collapse mode due to the activation of friction constraints; a mixed collapse behavior occurs for $0.3522 \le \tan\psi \le 0.3528$ and $0.3645 \le \tan\psi \le 0.3652$, respectively (see the sloped segment); a collapse mode involving only strength constraints is identified for $0.3528 \le \tan\psi \le 0.6$ and $0.3652 \le \tan\psi \le 0.6$, respectively (see the horizontal segment).

4.2. Dome

The funicular approach already used in two dimensions to investigate the structural behavior of the arch, is here applied, with no modification, to the dome. Both material A and material B are considered. Only the number of investigations per set of analyses that refer to the same value of $\tan\psi$ is reduced, to contain the computational burden and assess the validity of the proposed approach in achieving reasonable results with fewer tests.

In Fig. 16 normalized histograms are given for three different values of the friction coefficient, along with the adopted estimate of the probability density function. For large values of the friction coefficient, say $\tan\psi \ge 0.4$, the same log-normal density function may be used as an estimate of the PDF of the continuous random variable λ, see e.g. the case $\tan\psi = 0.45$ in Fig. 16(left). As it was for the reference log-normal distribution introduced in Section 4.1 to handle the random variable at large values of $\tan\psi$, this PDF will be further referred to as $g(\lambda)$, being $G(\lambda)$ the relevant CDF. For intermediate values of the friction coefficient, say $0.21 < \tan\psi < 0.4$, histograms of the type shown in Fig. 16(center) are found, which are bounded from above by a load multiplier λ_k that has relative occurrence equal to a_k. Eq. (13) is still adopted as a preliminary approximation of the (generalized) PDF of the mixed random variable in the intermediate range of the coefficient of friction. For the case depicted in Fig. 16(center), one has

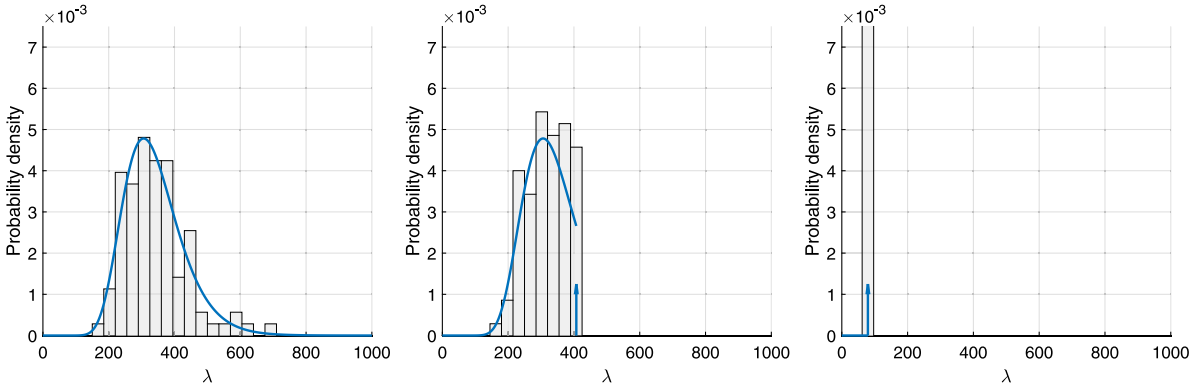

Fig. 16. Dome (material A). Normalized histogram and estimate of the probability density of the load multiplier for different values of the friction coefficient: $\tan\psi = 0.45$ (left), $\tan\psi = 0.35$ (center), and $\tan\psi = 0.2$ (right).

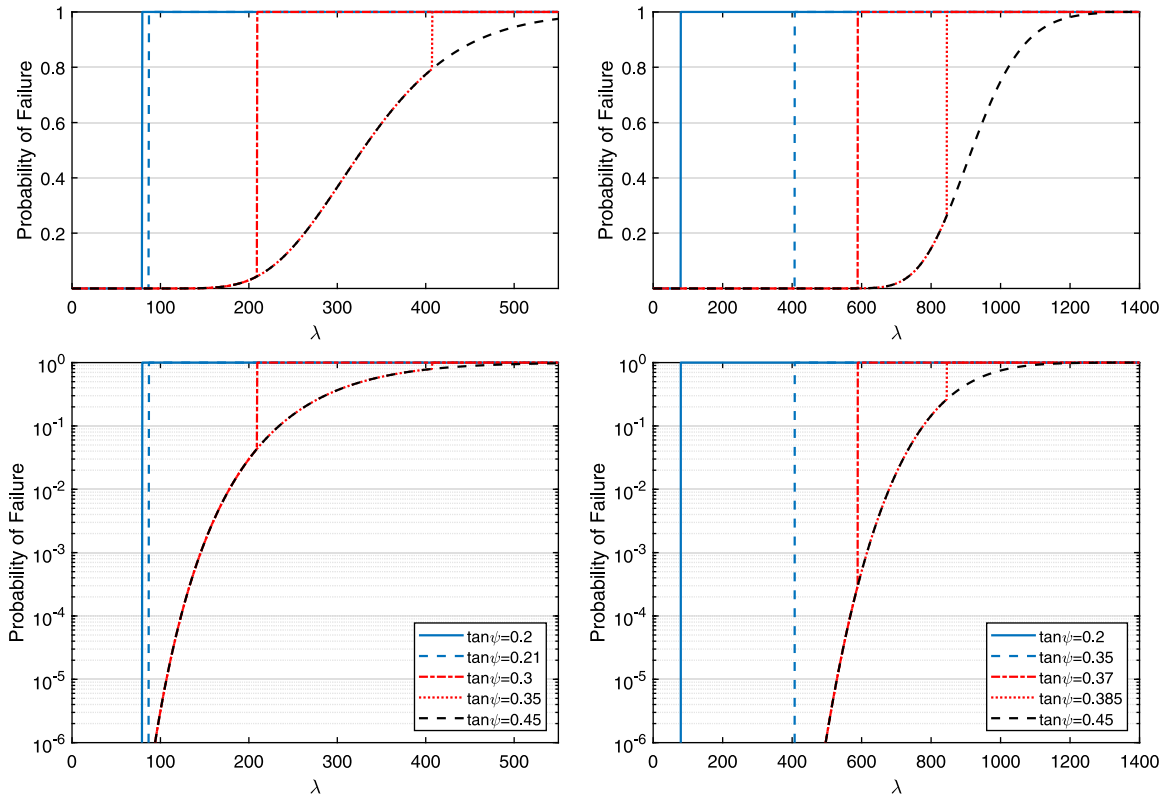

Fig. 17. Dome. Probability of failure vs. load multiplier for prescribed values of the friction coefficient: material A (left) and material B (right). The probability range is [0, 1] on top, whereas $[10^{-6}, 1]$ below.

$\lambda_k = 407.24$ and $a_k = 17/100$, with a scaling parameter $b_k = 0.206$. For small values of the friction coefficient, that means $\tan\psi \leq 0.21$, one load multiplier per coefficient is found. Again, Eq. (13) is used as the generalized PDF, which turns out to consist in the Dirac delta function $\delta(\lambda - \lambda_k)$. Indeed, in the case $\tan\psi = 0.2$ of Fig. 16(right), the whole set of simulations provides the value $\lambda_k = 79.33$. The relative occurrence $a_k = 1$, whereas the adopted scaling factor is $b_k \sim 1$.

Due to similarity of results between Figs. 16 and 7, diagrams reporting the probability of failure vs. the coefficient of friction for the dome exhibit the same features of those computed for the arch, see Fig. 17(left). For $\tan\psi \geq 0.4$, the probability of failure is not affected by the friction coefficient in any appreciable manner. When the coefficient of friction is too small, failure is a sure event for load multipliers that exceed a certain value, depending on $\tan\psi$, whereas the structure is safe below. This is the case of $\tan\psi = 0.2$: no equilibrium can be found at $\lambda > 79.33$; otherwise the probability of failure is negligible. In between, the diagrams

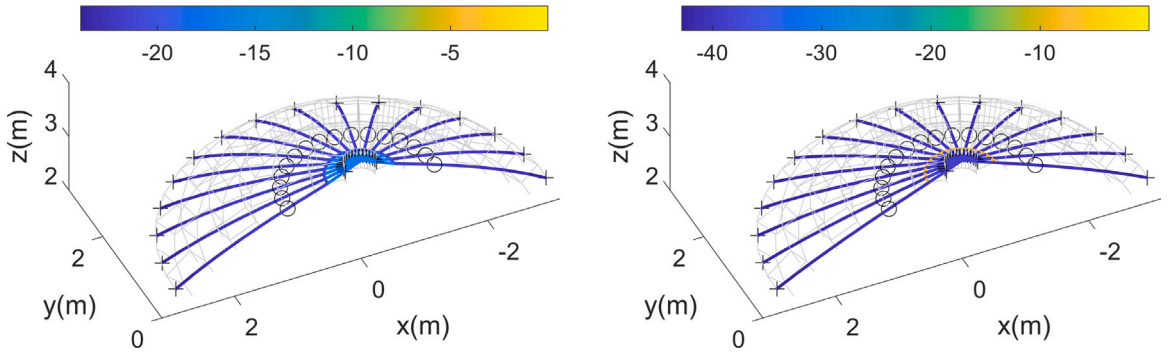

Fig. 18. Dome (material A). Funicular networks at incipient collapse for $\tan\psi = 0.45$ and: $\sigma_{cA,0.05}$ ($\lambda = 220.00$) (left) and $\sigma_{cA,0.95}$ ($\lambda = 465.30$) (right). Forces are in kN.

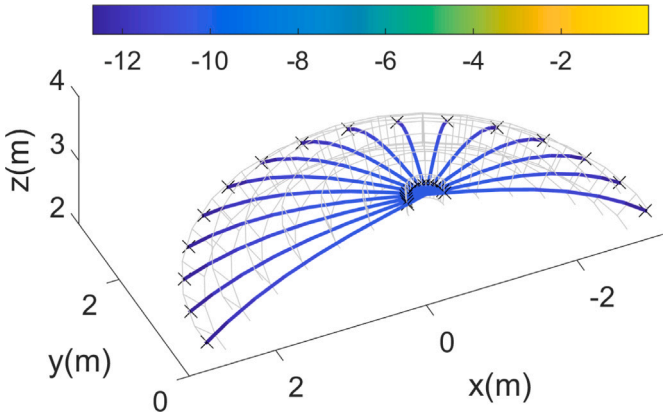

Fig. 19. Dome (material A). Funicular network at incipient collapse for $\tan\psi = 0.2$ and $\sigma_{cA,0.05}$ ($\lambda = 79.33$). Forces are in kN.

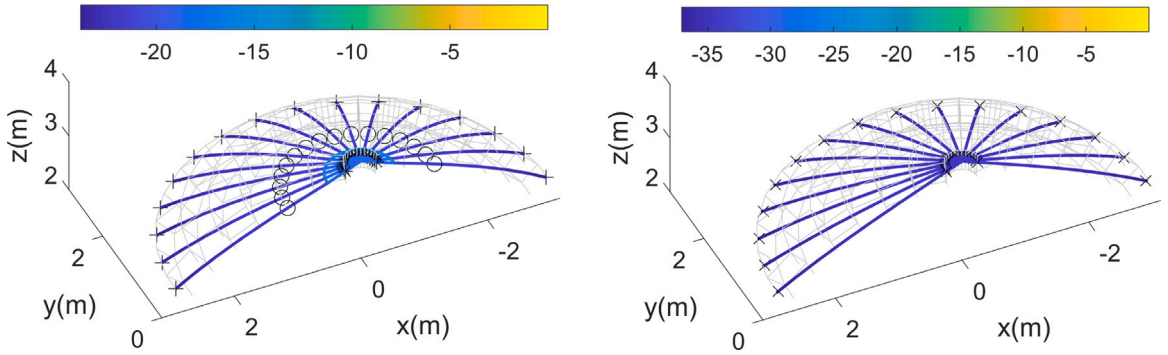

Fig. 20. Dome (material A). Funicular networks at incipient collapse for $\tan\psi = 0.35$ and: $\sigma_{cA,0.05}$ ($\lambda = 219.08$) (left) and $\sigma_{cA,0.95}$ ($\lambda = 407.24$) (right). Forces are in kN.

are made of a portion of the curve found for $\tan\psi \geq 0.4$, which undergoes an abrupt change at a location that strongly depends on $\tan\psi$. For instance, considering $\tan\psi = 0.35$, failure becomes a sure event at $\lambda > 407.24$. In Fig. 17(right), curves reporting the probability of failure vs. λ for different values of the coefficient of friction are given in the case of material B. As already seen for the arch, the behavior is exactly the same at very low values of $\tan\psi$, see curves for $\tan\psi = 0.2$. Again, the distribution of the compressive strength of material B generally allows for a noticeable increase in terms of load multipliers, for the same probability of failure, provided that no purely friction collapse occurs due to lack of frictional resistance.

Additional investigations are reported for the dome with material A, with the aim of assessing the link between collapse modes and statistics in Fig. 16. Funicular networks at incipient collapse are represented in Fig. 18 for the case of $\tan\psi = 0.45$, both for $\sigma_{cA,0.05}$ and $\sigma_{cA,0.95}$. Independently on the value of the compressive strength, the same joint sections where crossing members activate

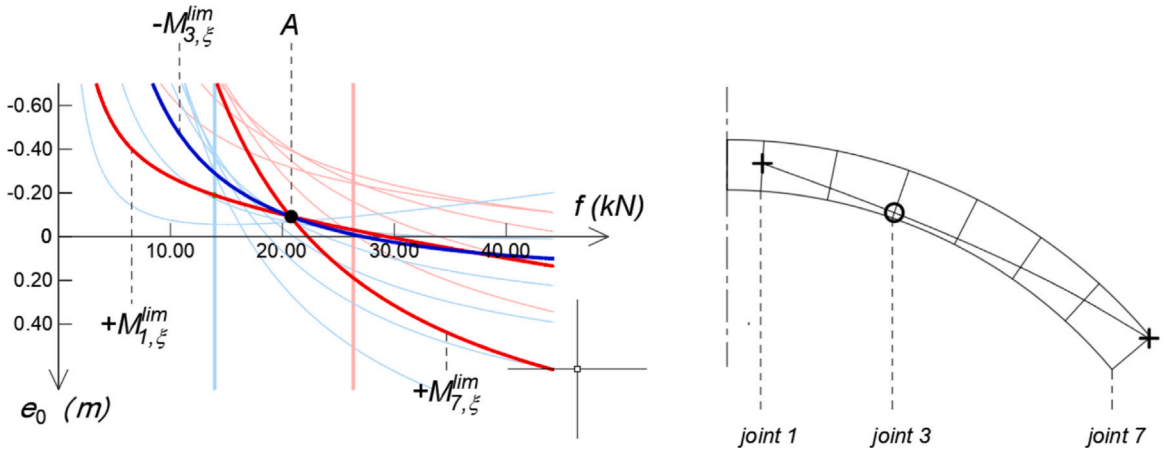

Fig. 21. Dome (material A). The stability area A reduces to a single point for $\tan\psi = 0.45$ and $\sigma_{cA,0.05}$ ($\lambda_{DC} = 222.17$) (left); the corresponding thrust line, with the location of the critical joints (right).

a strength constraint are responsible for the incipient activation of a collapse mode, whereas no Coulomb's friction constraint is active. The achieved funicular networks (involving all the meridians and the upper parallel) have the same geometry, but differ in terms of the associated load multiplier. As already observed for the arch, this confirms why for large values of $\tan\psi$, the continuous random variable λ may be handled through the same density function, see Fig. 16(left). When $\tan\psi = 0.2$, the solution retrieved for $\sigma_{cA,0.05}$ coincides with that found for $\sigma_{cA,0.95}$, see Fig. 19. The funicular network is made of meridians only, which activate friction constraints both at the crown and at the imposts. This case illustrates the description of λ as a discrete random variable, as done in Fig. 16(right). The last set of investigations refers to the case $\tan\psi = 0.35$, which falls in the range where λ behaves as a mixed random variable, see Fig. 16(center). For $\sigma_{cA,0.05}$ the retrieved funicular network looks like those found for $\tan\psi = 0.45$. Indeed, with respect to the solution in Fig. 18(left), the result in Fig. 20(left) is characterized by the additional activation of Coulomb's friction constraints at keystone, whereas the load multiplier is slightly lower. For $\sigma_{cA,0.95}$, a funicular polygon of the type already found for $\tan\psi = 0.2$ (but a larger value of the load multiplier) is reported, see Fig. 20(right) in comparison to Fig. 19.

To validate the above results, given the particular loading conditions and axial symmetry, the Durand-Claye method is exploited to evaluate the collapse load multiplier related to any of the 'lunes' composing the dome, according to the 'slicing technique'. By examining the associated mechanism, it is determined if the limit condition thus identified for a single 'lune' corresponds to the collapse of the entire dome [47].

The first dome under examination is that plotted in Fig. 18(left), along with the funicular network at incipient collapse. The friction angle and the compressive strength are $\tan\psi = 0.45$ and $\sigma_{cA,0.05}$, respectively, while the collapse load multiplier found through the funicular method is $\lambda = 220.00$, with a funicular networks made by all the meridians and the upper parallel. Working with meridians only, the collapse load multiplier retrieved by the funicular method is $\lambda = 212.66$, which corresponds to the same set of active failure constraints represented in Fig. 18(left). Because the parallels do not make a significant contribution in the considered case, the Durand-Claye method, which handles the single 'lune' without accounting for any hoop force, is used for validation purposes. For the first dome under examination, the stability area method provides the collapse load multiplier $\lambda_{DC} = 222.17$. Note that the stability area related to a single 'lune' shrinks to a single point (see the black point in Fig. 21, left), defined by the intersection between the curves $+M^{lim}_{1,\xi}$, $+M^{lim}_{7,\xi}$(red curves), and $-M^{lim}_{3,\xi}$ (blue curve). This point is contained in the sliding domain, identified by the region comprised between the two vertical straight lines belonging to the (f, e_0) plane: in this case, collapse depends only on the hypotheses on the strength of masonry, not on the coefficient of friction. In Fig. 21(right), the thrust line corresponding to incipient collapse is plotted, with the location of the centers of pressure at the critical joints. Full agreement with the network provided by the funicular method is reported.

For a very low value of the friction coefficient, $\tan\psi = 0.2$, the funicular network at incipient collapse ($\lambda = 79.33$) shows the activation of two friction constraints at joints $i = 1$ and $i = 7$ (Fig. 19). Durand-Claye's method confirms such a result. In Fig. 22(left) the collapse condition, corresponding to $\lambda_{DC} = 79.88$, is represented in the (f, e_0) plane. The stability area A is the black vertical segment, which identifies a unique value of the crown thrust, f, and an infinite set of thrust lines (Fig. 22, right). The critical joints, where the limit friction condition is attained, coincide with those provided by the funicular method, joint $i = 1$ (blue joint) and joint $i = 7$ (red joint).

Regarding the validation of the results, a brief remark on the modeling of the ith joint is given here, with a specific reference to the case studies plotted in Fig. 18. As described in Section 3, according to the modern version of Durand-Claye's method for masonry domes, any joint is schematized as a rectangle of dimensions $l_{i,\eta} \times x_{C_i} \Delta\phi$ (see Fig. 3). In the funicular method, conversely, a different procedure is adopted, which identifies the maximum rectangle inscribed inside the joint. Despite these slightly different assumptions on the joint's shape, the results related to the domes obtained using the two methods are in good agreement (as testified by the examples described above).

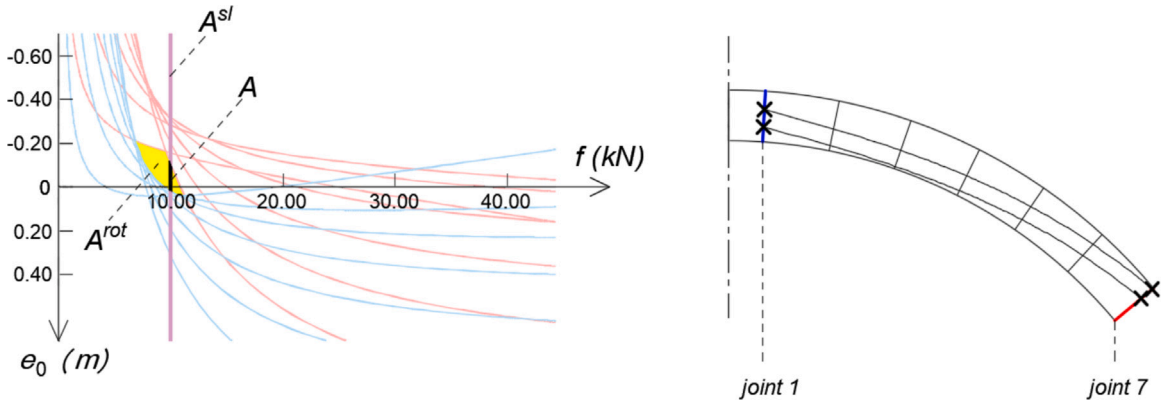

Fig. 22. Dome (material A). The stability area A reduces to a segment for $\tan\psi = 0.2$ and $\sigma_{cA,0.05}$ ($\lambda_{DC} = 79.88$) (left); the corresponding set of thrust lines, with the location of the critical joints (right).

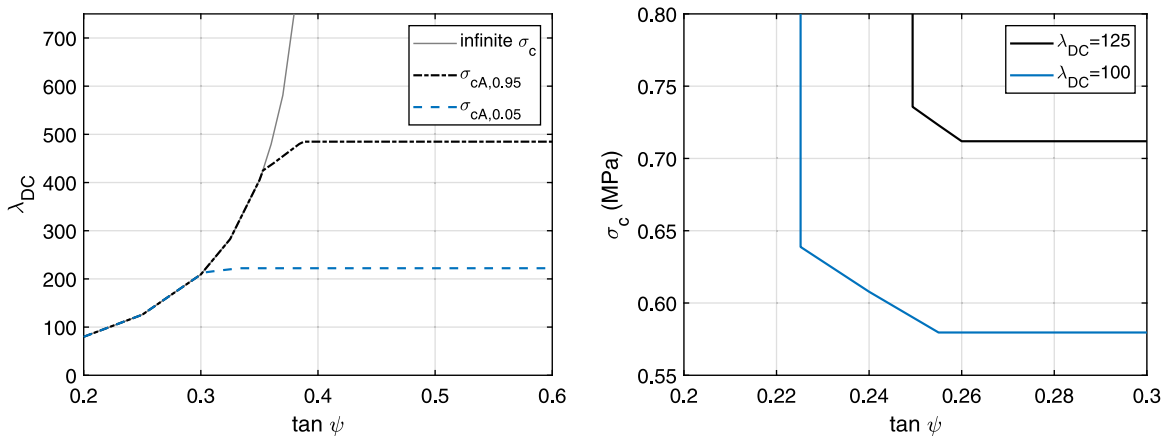

Fig. 23. Dome (material A). Maximum load multiplier, λ_{DC} *versus* friction coefficient, $\tan\psi$, for assigned values of the compressive strength (left); compressive strength corresponding to an incipient collapse condition, σ_c, *versus* friction coefficient, $\tan\psi$, for assigned values of λ_{DC} (right).

It is interesting to remark that for both domes in Fig. 18, due to the three-dimensional modeling provided by the funicular method, the collapse condition is characterized not only by the activation of strength constraints at three critical joints, but also by the presence of a compressed parallel. This result, which deserves further investigation, is linked to the hypothesis of a limited compressive strength and cannot be retrieved by the 'slicing technique', which does not capture the effects of the internal forces along the parallels in the condition of incipient collapse. Given the above, the value of the collapse load multiplier determined through the Durand-Claye method (based on the 'slicing technique') should be lower than that obtained by means of the funicular method, capable of taking into account the three-dimensional behavior of the dome. This does not occur when the ith joint is schematized as described in Section 3. On the contrary, considering a rectangle of dimensions $l_{i,\eta} \times x_{D_i} \Delta\phi$ (i.e. a slightly smaller rectangle, in favor of safety) provides even better consistency with the results obtained via the funicular method: $\lambda_{DC} = 212.59$ for the first dome, while $\lambda_{DC} = 464.65$ for the second dome. Both values of λ_{DC} are close to those obtained with the funicular method implementing a full three-dimensional network ($\lambda = 220.00$ and $\lambda = 465.30$), but are lower than them, in accordance with the mechanical models underlying the two methods, respectively. Also, they are in full agreement with the collapse load multipliers obtained with the funicular method implementing meridians only, i.e. $\lambda = 212.66$ and $\lambda = 464.74$, respectively.

As already done for arches, deterministic analyses are performed by means of Durand-Claye's method in order to study the collapse of masonry domes. In Fig. 23(left), the collapse load multiplier, λ_{DC}, is plotted *versus* the friction coefficient, by assuming constant values for the compressive strength. By fixing $\sigma_c = \sigma_{cA,0.05} = 1.26$ MPa (resp. $\sigma_{cA,0.95} = 3.07$ MPa), three different collapse modes are identified: a collapse mode involving the activation of friction constraints for $0.2 \leq \tan\psi \leq 0.302$ (resp. $0.2 \leq \tan\psi \leq 0.353$); a mixed collapse mode (corresponding to the activation of both friction and strength constraints) for $0.302 \leq \tan\psi \leq 0.333$ (resp. $0.353 \leq \tan\psi \leq 0.388$); a collapse mode involving only the activation of no-tension/crushing constraints for $0.333 \leq \tan\psi \leq 0.6$ (resp. $0.388 \leq \tan\psi \leq 0.6$). The transition between a sliding collapse mode and a rotational collapse mode occurs over a wider (although still narrow) range of friction coefficients than that found in the arches examined. Again, the initial part of the curves drawn for $\sigma_c = \sigma_{cA,0.05}$ and $\sigma_c = \sigma_{cA,0.95}$ lies along that found when considering infinite compressive strength.

In Fig. 23(right), the compressive strength corresponding to an incipient collapse condition is determined, by assuming that the collapse load multiplier is assigned ($\lambda_{DC} = 100$ and $\lambda_{DC} = 125$), while the friction coefficient, $\tan\psi$, varies. The graph is composed of a vertical segment, corresponding to the value of the friction coefficient that identifies a purely sliding collapse mode, $\tan\psi = 0.2252$ for $\lambda_{DC} = 100$, $\tan\psi = 0.2494$ for $\lambda_{DC} = 125$. For $0.2252 \leq \tan\psi \leq 0.2550$ ($\lambda_{DC} = 100$) and $0.2494 \leq \tan\psi \leq 0.2600$ ($\lambda_{DC} = 125$) mixed collapse modes arise: the sloped segment provides the limit value of the compressive strength *versus* the friction coefficient. Finally, a collapse mode involving only strength constraints occurs for $0.2550 \leq \tan\psi \leq 0.6$ ($\lambda_{DC} = 100$) and $0.2600 \leq \tan\psi \leq 0.6$ ($\lambda_{DC} = 125$). Also in this case, the examples of domes here considered exhibit a behavior characterized by a less abrupt transition between sliding and rotational collapse modes.

The impact of a limited compressive strength and/or finite friction on the collapse behavior of masonry arches has been addressed from a deterministic perspective particularly in [32,35]. More in detail, analyses aimed at defining the minimum thickness in the hypothesis of finite strength and finite friction have been addressed in [35], whereas the effects of friction together with other parameters have been investigated in [32]. A common denominator of the above mentioned deterministic approaches, which include the investigations based on the stability area method herein described, is the identification of different collapse modes depending on the value of the friction coefficient. Collapse due to the arising of hinges or to the activation of strength constraints is realistic, provided that friction can prevent sliding between the voussoirs; otherwise, by progressively decreasing the friction coefficient, mixed and purely sliding collapse modes occur. The probabilistic approach presented in this paper aims at enriching the framework of the deterministic procedures by taking into account uncertainties on the mechanical parameters. Collapse modes retrieved at varying friction coefficients are in agreement with trends outlined by the referenced deterministic literature.

5. Conclusions and ongoing research

A numerical investigation has been performed to assess the structural behavior of masonry arches and domes taking into account a finite friction and a finite compressive strength of the material. Based on the availability of probabilistic models in the literature, the finite compressive strength has been considered uncertain, adopting log-normal distributions suggested by technical documents [48], whereas the impact of the friction coefficient has been assessed spanning a reasonable range related to the finishing of the voussoirs [49] and exploiting the concept of fragility curves.

The main aim of the paper is providing a simple probabilistic approach to support performance assessment and risk analysis of blocky stone structures, which are peculiar of historical constructions. For a given type of brickwork that is affected by uncertainties on strength, fragility curves are shown to give a straightforward description of the expected collapse behavior.

More in details, Monte Carlo simulations have been performed for several samples of the compressive strength, repeating the investigation for a discrete set of angles of friction. An arch and a dome with conventional stereotomy have been investigated to demonstrate the procedure, considering self-weight and a live point load applied at the crown. Each one of the analyses has been performed by solving a maximization problem that has been conceived for obtaining the maximum static load multiplier of the live load, given a friction coefficient and a compressive strength. The method combines funicular analysis operated by the force density method and sequential convex programming, enforcing constraints on the normal and shear resultants of the stresses at each joint. The implemented algorithm has been validated by means of the Durand-Claye's semi-analytical method: in this case, an iterative procedure has been adopted to find the load multiplier corresponding to the limit condition, i.e., to the vanishing of the stability area.

For each one of the considered values of the friction coefficient, the output random variable, i.e. the computed load multiplier, has been analyzed. For large values of the friction coefficient, the load multiplier behaves as a continuous random variable whose distribution is not affected by $\tan\psi$. This is related to the arising of a limit condition that does not involve the activation of friction constraints. Conversely, for low values of the friction coefficient, the output random variables practically behaves as a discrete one. Independently on the compressive strength, all the discrete simulations converge to the same load multiplier. The limit condition is related to the activation of a failure mode that is purely frictional. In between, a mixed random variable is retrieved. The upper tail of the continuous part is truncated by the localization of a subset of the results at a bounding value. Limit conditions that are purely frictional, or related to the activation of strength constraints only, are mostly found, retrieving collapse modes that have been already encountered for small and large values of $\tan\psi$, respectively. Indeed, as a preliminary approximation, the same distribution already used at large values of the friction coefficient has been retained to build the truncated parts in the intermediate range.

By post-processing the achieved results, the probability of failure related to the load multipliers has been investigated across $\tan\psi$. It was found that diagrams of the type failure probability vs. load multipliers are not affected in any appreciable manner by the coefficient of friction only for large values of $\tan\psi$. In the intermediate and lower range, a certain value of $\tan\psi$ exists below which the probability of failure blows up, being related to the occurrence of purely frictional collapse modes. The probabilistic investigation has been performed for two different kinds of brickwork, i.e. ashlars of soft stone, and stone square blocks. Both for the arch and the dome, the latter material generally allows for a remarkable increase in the values of the load multiplier pertaining to similar probabilities of failure. This holds, provided that the friction coefficient is such as to avoid the occurrence of purely friction collapse. Indeed, the behavior is exactly the same for very low values of $\tan\psi$.

It must be remarked that symmetrically loaded structures have been considered to safely apply the lower bound theorem in the case of finite friction. This also allowed for neglecting torsion-related failure modes and for providing a cross-validation of the funicular approach and the stability area method. In fact, the main limitation of the proposed approach resides in the type of blocky structures that can be affordably investigated. Peculiar attention should be paid to the assumption made on the estimate of the continuous part of the probability distribution for the load multipliers, i.e. the adoption of the same function all over the range of

the friction coefficients. Further research is needed to improve the accuracy of the achieved results, especially in the intermediate range of the friction coefficients. A more precise estimation of the output random variable could be conveniently performed, also investigating the impact of mixed failure modes. Hence, the role of stereotomy could be assessed, by testing several types of geometry of the blocks.

Among the others, construction defects, deterioration of materials over time and occurrence of seismic events introduce spatial variations in the strength of the material, see in particular [66]. The ongoing research is also focused in the adoption of random fields to account for such kind of uncertainties, see e.g. [67]. An additional topic of research is concerned with the extension of the proposed optimization problem, originally conceived for the limit analysis of unreinforced arches and domes, to the design of their optimal strengthening under the effect of uncertainties, see e.g. [68–70].

CRediT authorship contribution statement

Danila Aita: Writing – review & editing, Writing – original draft, Validation, Methodology, Formal analysis, Conceptualization. **Matteo Bruggi:** Writing – review & editing, Writing – original draft, Software, Methodology, Formal analysis, Conceptualization. **Elsa Garavaglia:** Writing – review & editing, Writing – original draft, Methodology, Formal analysis, Data curation, Conceptualization.

Declaration of competing interest

The authors declare that they have no known competing financial interests or personal relationships that could have appeared to influence the work reported in this paper.

Data availability

Data will be made available on request.

References

[1] P.B. Lourenço, G. Milani, Homogenization and seismic assessment: Review and recent trends, in: CISM International Centre for Mechanical Sciences, in: Courses and Lectures, vol. 551, 2014, pp. 293–341.
[2] J. Pina-Henriques, P.B. Lourenço, Masonry compression: a numerical investigation at the meso-level, Eng. Comput. 23 (2006) 382–407.
[3] E. Sassoni, C. Mazzotti, G. Pagliai, Comparison between experimental methods for evaluating the compressive strength of existing masonry buildings, Constr. Build. Mater. 68 (2014) 206–219.
[4] P.M. Naik, T. Bhowmik, A. Menon, Estimating joint stiffness and friction parameters for dry stone masonry constructions, Int. J. Mason. Res. Innov. 6 (2) (2021) 232–254.
[5] A. Anzani, E. Garavaglia, L. Binda, Long-term damage of historic masonry: A probabilistic model, Constr. Build. Mater. 23 (2) (2009) 713–724.
[6] E. Garavaglia, R. Pavani, L. Sgambi, Fragility curves as a handy forecasting method, in: AIP Conference Proceedings, Vol. 2849, 2023, pp. 1–4, 040002.
[7] S. Saloustros, L. Pelà, F.R. Contrafatto, P. Roca, I. Petromichelakis, Analytical derivation of seismic fragility curves for historical masonry structures based on stochastic analysis of uncertain material parameters, Int. J. Archit. Heritage 13 (7) (2019) 1142–1164.
[8] L.C. da Silva, G. Milani, P.B. Lourenço, Probabilistic-based discrete model for the seismic fragility assessment of masonry structures, Structures 52 (2023) 506–523.
[9] N. Cavalagli, V. Gusella, R. Liberotti, Effect of shape uncertainties on the collapse condition of the circular masonry arch, Adv. Struct. Mater. 130 (2020) 455–467.
[10] B. Ghiassi, P.B. Lourenço, Long-term Performance and Durability of Masonry Structures: Degradation Mechanisms, Health Monitoring and Service Life Design, Woodhead Publishing, 2018, pp. 1–404.
[11] R. Bento, G. Milani, M. Mosoarca, V. Sarhosis, Failure analysis of existing structures and infrastructures under extreme events and long-term actions, Eng. Fail. Anal. 156 (2024).
[12] J. Simon, K. Bagi, Discrete element analysis of the minimum thickness of oval masonry domes, Int. J. Archit. Heritage 10 (4) (2016) 457–475.
[13] R. Bravo, J. Pérez-Aparicio, Combined finite–discrete element method for parameter identification of masonry structures, Constr. Build. Mater. 396 (2023).
[14] G.L.S. Sacco, C. Ferrero, C. Battini, C. Calderini, Combined use of deformation and structural analysis for the structural damage assessment of heritage buildings: A case study in the liguria region (Italy), Eng. Fail. Anal. 147 (2023).
[15] M. Bruggi, A constrained force density method for the funicular analysis and design of arches, domes and vaults, Int. J. Solids Struct. 193–194 (2020) 251–269.
[16] Y. Hua, G. Milani, Simple modeling of reinforced masonry arches for associated and non-associated heterogeneous limit analysis, Comput. Struct. 280 (2023).
[17] D. Aita, G. Milani, A. Taliercio, Limit analysis of masonry domes with oculus and lantern: A comparison between different approaches, Math. Mech. Solids (2023).
[18] M. Angelillo, P.B. Lourenço, G. Milani, Masonry behaviour and modelling, in: CISM International Centre for Mechanical Sciences, in: Courses and Lectures, vol. 551, 2014, pp. 1–26.
[19] J. Heyman, The stone skeleton, Int. J. Solids Struct. 2 (2) (1966) 249–279.
[20] S. Galassi, G. Misseri, L. Rovero, G. Tempesta, Equilibrium analysis of masonry domes. on the analytical interpretation of the Eddy-Lévy graphical method, Int. J. Archit. Heritage 11 (8) (2017) 1195–1211.
[21] P. Block, J. Ochsendorf, Thrust network analysis: A new methodology for three-dimensional equilibrium, J. Int. Assoc. Shell Spat. Struct. 48 (155) (2007) 167–173.
[22] F. Fraternali, A thrust network approach to the equilibrium problem of unreinforced masonry vaults via polyhedral stress functions, Mech. Res. Commun. 37 (2) (2010) 198–204.
[23] M. Angelillo, A. Fortunato, A. Montanino, M. Lippiello, Singular stress fields in masonry structures: Derand was right, Meccanica 49 (5) (2014) 1243–1262.
[24] A. Gesualdo, C. Cennamo, A. Fortunato, G. Frunzio, M. Monaco, M. Angelillo, Equilibrium formulation of masonry helical stairs, Meccanica 52 (8) (2017) 1963–1974.

[25] A. Montanino, D. De Gregorio, C. Olivieri, A. Iannuzzo, The continuous airy-based for stress-singularities (CASS) method: an energy-based numerical formulation for unilateral materials, Int. J. Solids Struct. 256 (2022) 111954.
[26] N. Nodargi, P. Bisegna, Minimum thrust and minimum thickness of spherical masonry domes: A semi-analytical approach, Eur. J. Mech. A Solids 87 (2021).
[27] N. Nodargi, P. Bisegna, A new computational framework for the minimum thrust analysis of axisymmetric masonry domes, Eng. Struct. 234 (2021).
[28] N. Nodargi, An isogeometric collocation method for the static limit analysis of masonry domes under their self-weight, Comput. Methods Appl. Mech. Engrg. 416 (2023).
[29] A. Sinopoli, Unilaterality and dry friction: A geometric formulation for two-dimensional rigid body dynamics, Nonlinear Dynam. 12 (4) (1997) 343–366.
[30] D. Aita, A. Sinopoli, Two different approaches for collapse of nonsymmetric masonry arches: Monasterio's treatment versus limit equilibrium analysis, J. Eng. Mech. 147 (10) (2021).
[31] G. Cocchetti, E. Rizzi, Analytical and numerical analysis on the collapse modes of least-thickness circular masonry arches at decreasing friction, Fract. Struct. Integr. 14 (51) (2020) 356–375.
[32] B. Nela, M. Pingaro, P. Trovalusci, M. Pasca, Limit analysis of multi-ring masonry arches: a parametric study on the effects of friction angle, geometry, interlocking, and ring number, Front. Built Environ. 9 (2023).
[33] M. Fantin, T. Ciblac, Extension of thrust network analysis with joints consideration and new equilibrium states, Int. J. Space Struct. 31 (2–4) (2016) 190–202.
[34] N.A. Nodargi, P. Bisegna, Generalized thrust network analysis for the safety assessment of vaulted masonry structures, Eng. Struct. 270 (2022) 114878.
[35] A. Caporale, R. Luciano, Limit analysis of masonry arches with finite compressive strength and externally bonded reinforcement, Composites B 43 (8) (2012) 3131–3145.
[36] D. Aita, R. Barsotti, S. Bennati, Looking at the collapse modes of circular and pointed masonry arches through the lens of Durand–Claye's stability area method, Arch. Appl. Mech. 89 (8) (2019) 1537–1554.
[37] D.C. Drucker, Limit analysis of two and three dimensional soil mechanics problems, J. Mech. Phys. Solids 1 (4) (1953) 217–226.
[38] D. Radenkovic, Théorèmes limites pour un materiau de Coulomb à dilatiation non standardisée, C. R. l'Acad. Sci. 252 (1961) 4103–4104.
[39] R.K. Livesley, Limit analysis of structures formed from rigid blocks, Internat. J. Numer. Methods Engrg. 12 (12) (1978) 1853–1871.
[40] T.E. Boothby, Stability of masonry piers and arches including sliding, J. Eng. Mech. 120 (2) (1994) 304–319.
[41] C. Baggio, P. Trovalusci, Collapse behaviour of three-dimensional brick-block systems using non-linear programming, Struct. Eng. Mech. 10 (2) (2000) 181–195.
[42] C. Casapulla, Dry rigid block masonry: Safe solutions in presence of Coulomb friction, WIT Trans. Built Environ. 55 (2001) 251–261.
[43] D. D'Ayala, C. Casapulla, Limit state analysis of hemispherical domes with finite friction, in: P.B. Lourenço, P. Roca (Eds.), Proceedings of the 3rd International Conference Structural Analysis of Historical Constructions, 2001, pp. 617–626.
[44] H. Schek, The force density method for form finding and computation of general networks, Comput. Methods Appl. Mech. Engrg. 3 (1) (1974) 115–134.
[45] D. Aita, M. Bruggi, A numerical method for the funicular analysis of masonry vaults accounting for stereotomy, finite strength and finite friction, Eng. Struct. 293 (2023) 116658.
[46] D. Aita, R. Barsotti, S. Bennati, Equilibrium of pointed, circular, and elliptical masonry arches bearing vertical walls, J. Struct. Eng. 138 (7) (2012) 880–888.
[47] D. Aita, R. Barsotti, S. Bennati, Studying the dome of Pisa cathedral via a modern reinterpretation of Durand–Claye's method, J. Mech. Mater. Struct. 14 (2019) 603–619.
[48] CNR, Guide for the Probabilistic Assessment of the Seismic Safety of Existing Buildings, Technical Document CNR-DT 212/2013, 2014, pp. 24–25.
[49] P.B. Lourenço, L.F. Ramos, Characterization of cyclic behavior of dry masonry joints, J. Struct. Eng. 130 (5) (2004) 695–827.
[50] R.P. Kennedy, C.A. Cornell, R.D. Campbell, S. Kaplan, H.F. Perla, Probabilistic seismic safety study of an existing nuclear power plant, Nucl. Eng. Des. 59 (2) (1980) 315–338.
[51] D. O'Dwyer, Funicular analysis of masonry vaults, Comput. Struct. 73 (1–5) (1999) 187–197.
[52] P. Block, L. Lachauer, Three-dimensional funicular analysis of masonry vaults, Mech. Res. Commun. 56 (2014) 53–60.
[53] A. Liew, R. Avelino, V. Moosavi, T. Van Mele, P. Block, Optimising the load path of compression-only thrust networks through independent sets, Struct. Multidiscip. Optim. 60 (1) (2019) 231–244.
[54] M. Bruggi, B. Lógó, Z. Deák, Funicular analysis of ribbed masonry vaults: A case study, Int. J. Archit. Heritage 16 (12) (2022) 1809–1823.
[55] C.A. Coulomb, Essai sur une application des règles de maximis et minimis à quelques problèmes de statique, relatifs à l'architecture, mémoires de mathématique et de physique, in: Académie Royale des Sciences par Divers Savans, 1776, pp. 343–382.
[56] C. Baggio, P. Trovalusci, Limit analysis for no-tension and frictional three-dimensional discrete systems, Mech. Struct. Mach. 26 (3) (1998) 287–304.
[57] A. Orduña, P.B. Lourenço, Three-dimensional limit analysis of rigid blocks assemblages. Part I: Torsion failure on frictional interfaces and limit analysis formulation, Int. J. Solids Struct. 42 (18–19) (2005) 5140–5160.
[58] M. Bruggi, V. Laghi, T. Trombetti, Stress-based form-finding of gridshells for wire-and-arc additive manufacturing considering overhang constraints, Eng. Struct. 279 (2023) 115654.
[59] K. Svanberg, The method of moving asymptotes—a new method for structural optimization, Internat. J. Numer. Methods Engrg. 24 (2) (1987) 359–373.
[60] A. Durand-Claye, Note sur la vérification de la stabilité des voûtes en maçonnerie et sur l'emploi des courbes de pression, Ann. Ponts Chaussées 13 (1867) 63–93.
[61] A. Durand-Claye, Vérification de la stabilité des voûtes et des arcs. Applications aux voûtes sphériques, Ann. Ponts Chaussées 19 (1880) 416–440.
[62] J. Heyman, Equilibrium of Shell Structures, Oxford University Press, Oxford, UK, 1977.
[63] M. Como, Statics of Historic Masonry Constructions, in: Solid and Structural Mechanics, Springer, Cham, Swizerland, 2017.
[64] The MathWorks Inc., MATLAB Version: 9.13.0 (R2022b), The MathWorks Inc., Natick, Massachusetts, United States, 2022, Available from: https://www.mathworks.com.
[65] Wolfram Research Inc., Mathematica Version: 13.2, Wolfram Research Inc., Champaign, Illinois, United States, 2022, Available from: https://www.wolfram.com/mathematica.
[66] G. Milani, P.B. Lourenço, Monte Carlo homogenized limit analysis model for randomly assembled blocks in-plane loaded, Comput. Mech. 46 (6) (2010) 827–849.
[67] V. Gusella, F. Cluni, Random field and homogenization for masonry with nonperiodic microstructure, J. Mech. Mater. Struct. 1 (2) (2006) 357–386.
[68] F. Fraternali, G. Carpentieri, M. Modano, F. Fabbrocino, R. Skelton, A tensegrity approach to the optimal reinforcement of masonry domes and vaults through fiber-reinforced composite materials, Compos. Struct. 134 (2015) 247–254.
[69] M. Bruggi, A. Taliercio, Optimal strengthening of no–tension structures with externally bonded reinforcing layers or ties, Struct. Multidiscip. Optim. 55 (5) (2017) 1831–1846.
[70] I.H. Tarhan, H. Uysal, Topology optimization of the FRP for strengthening of masonry barrel vaults, Eng. Fail. Anal. 151 (2023) 107390.